



Evaluation of lipid biomarkers as proxies for sea ice and ocean temperatures along the Antarctic continental margin

Nele Lamping¹, Juliane Müller^{1,2,3}, Jens Heffter¹, Gesine Mollenhauer^{1,2,3}, Christian Haas¹, Xiaoxu Shi¹, Maria-Elena Vorrath¹, Gerrit Lohmann^{1,3,4}, and Claus-Dieter Hillenbrand⁵

¹Alfred Wegener Institute, Helmholtz Centre for Polar and Marine Research, 27568 Bremerhaven, Germany

²Department of Geosciences, University of Bremen, 28359 Bremen, Germany

³MARUM – Center for Marine Environmental Sciences, 28359 Bremen, Germany

⁴Department of Environmental Physics, University of Bremen, 28359 Bremen, Germany

⁵British Antarctic Survey, High Cross, Cambridge CB3 0ET, UK

Correspondence: Nele Lamping (nele.lamping@awi.de)

Received: 25 February 2021 – Discussion started: 1 March 2021

Revised: 9 September 2021 – Accepted: 13 September 2021 – Published: 29 October 2021

Abstract. The importance of Antarctic sea ice and Southern Ocean warming has come into the focus of polar research during the last couple of decades. Especially around West Antarctica, where warm water masses approach the continent and where sea ice has declined, the distribution and evolution of sea ice play a critical role in the stability of nearby ice shelves. Organic geochemical analyses of marine seafloor surface sediments from the Antarctic continental margin allow an evaluation of the applicability of biomarker-based sea-ice and ocean temperature reconstructions in these climate-sensitive areas. We analysed highly branched isoprenoids (HBIs), such as the sea-ice proxy IPSO₂₅ and phytoplankton-derived HBI-trienes, as well as phytosterols and isoprenoidal glycerol dialkyl glycerol tetraethers (GDGTs), which are established tools for the assessment of primary productivity and ocean temperatures respectively. The combination of IPSO₂₅ with a phytoplankton marker (i.e. the PIPSO₂₅ index) permits semi-quantitative sea-ice reconstructions and avoids misleading over- or underestimations of sea-ice cover. Comparisons of the PIPSO₂₅-based sea-ice distribution patterns and TEX₈₆^L- and RI-OH'-derived ocean temperatures with (1) sea-ice concentrations obtained from satellite observations and (2) instrument measurements of sea surface and subsurface temperatures corroborate the general capability of these proxies to determine oceanic key variables properly. This is further supported by model data. We also highlight specific aspects and limitations that need to be taken into account for the interpretation

of such biomarker data and discuss the potential of IPSO₂₅ as an indicator for the former occurrence of platelet ice and/or the export of ice-shelf water.

1 Introduction

One of the key components of the global climate system, influencing major atmospheric and oceanic processes, is floating on the ocean's surface at high latitudes – sea ice (Thomas, 2017). Southern Ocean sea ice is one of the most strongly changing features of the Earth's surface, as it experiences considerable seasonal variability with the sea-ice extent decreasing from a maximum of 20×10^6 km² in September to a minimum of 4×10^6 km² in March (Arrigo et al., 1997; Zwally, 1983). This seasonal waxing and waning of sea ice substantially modifies deep-water formation, influences the ocean–atmosphere exchange of heat and gas, and strongly affects surface albedo and radiation budgets (Abernathey et al., 2016; Nicholls et al., 2009; Turner et al., 2017). Moreover, sea ice regulates ocean buoyancy flux, upwelling and primary production (Schofield et al., 2018).

Based on the 40-year satellite record, the Southern Ocean sea-ice extent generally followed an increasing trend (Comiso et al., 2017; Parkinson and Cavalieri, 2012), experiencing an abrupt reversal from ca. 2015 to 2018 (Parkinson, 2019; Turner et al., 2020; Wang et al., 2019), which has been attributed to a multi-decadal oceanic warming and

the increased advection of atmospheric heat (Eayrs et al., 2021). However, the sea-ice extent around major parts of West Antarctica has been decreasing over the last 40 years (Parkinson and Cavalieri, 2012). The Antarctic Peninsula is particularly affected by a significant reduction in sea-ice extent and rapid atmospheric and oceanic warming (Etourneau et al., 2019; Li et al., 2014; Massom et al., 2018; Vaughan et al., 2003). The Larsen A and B ice shelves on the east coast of the Antarctic Peninsula collapsed in 1995 and 2002 respectively. These collapses were triggered by the loss of a sea-ice buffer, which enabled an increased flexure of the ice-shelf margins by ocean swell (Massom et al., 2018). Along the Pacific margin of West Antarctica, the Amundsen and Bellingshausen seas have also been affected by major sea-ice decline and regional surface ocean warming (Hobbs et al., 2016; Parkinson, 2019). Marine-terminating glaciers draining into the Amundsen and Bellingshausen seas are thinning at an alarming rate, which has been linked to sub-ice-shelf melting caused by relatively warm Circumpolar Deep Water (CDW) incursions into sub-ice-shelf cavities (e.g. Jacobs et al., 2011; Khazendar et al., 2016; Nakayama et al., 2018; Rignot et al., 2019; Smith et al., 2017). The disintegration of ice shelves reduces the buttressing effect that they exert on ice grounded further upstream, which can lead to partial or total loss of the ice in the catchments of the affected glaciers and, thus, raise global sea level considerably (3.4 to 4.4 m in case of a total West Antarctic Ice Sheet collapse) (Fretwell et al., 2013; Jenkins et al., 2018; Pritchard et al., 2012; Vaughan, 2008).

State-of-the-art climate models are not yet fully able to depict sea-ice seasonality and sea-ice cover, which the Fifth Assessment Report of the Intergovernmental Panel on Climate Change (Stocker et al., 2013) attributes to a lack of validation efforts using proxy-based sea-ice reconstructions. Hence, knowledge about (palaeo-) sea-ice conditions and ocean temperatures in the climate-sensitive areas around the West Antarctic Ice Sheet is considered to be crucial for understanding past and future climate evolution.

To date, the most common proxy-based sea-ice reconstructions in the Southern Ocean utilize fossil assemblages of sympagic (i.e. living within sea ice) diatoms preserved within the seafloor sediments (Allen et al., 2011; Armand and Leventer, 2003; Crosta et al., 1998; Esper and Gersonde, 2014; Gersonde and Zielinski, 2000; Leventer, 1998). Dissolution effects within the water column or after deposition, however, determine the preservation of small, lightly silicified diatom taxa and can, therefore, alter the assemblage record, leading to inaccurate sea-ice reconstructions (Leventer, 1998; Zielinski et al., 1998). Recently, the molecular remains of certain diatom taxa, i.e. specific organic geochemical lipids, have emerged as a potential proxy for reconstructing past Antarctic sea-ice cover (Barbara et al., 2013; Collins et al., 2013; Crosta et al., 2021; Denis et al., 2010; Etourneau et al., 2013; Lamping et al., 2020; Massé et al., 2011; Vorrath et al., 2019, 2020). Specifically, a di-unsaturated highly

branched isoprenoid (HBI) alkene (HBI diene, C_{25:2}) has been detected in both sea-ice diatoms from the Southern Ocean and Antarctic marine sediments (Johns et al., 1999; Massé et al., 2011; Nichols et al., 1988). Recently, the sympagic diatom *Berkeleya adeliensis*, which preferably proliferates in platelet ice, has been identified as the producer of this HBI alkene (Belt et al., 2016; Riaux-Gobin and Poulin, 2004). However, *B. adeliensis* seems rather flexible concerning its habitat, as it has also been recorded in the bottom ice layer and is apparently well adapted to changes in texture during ice melt (Riaux-Gobin et al., 2013). Belt et al. (2016) introduced the term IPSO₂₅ (Ice Proxy of the Southern Ocean with 25 carbon atoms) by analogy to its counterpart IP₂₅ in the Arctic. Commonly, for a more detailed assessment of sea-ice conditions, IP₂₅ in the Arctic Ocean and IPSO₂₅ in the Southern Ocean have been measured alongside complementary phytoplankton-derived lipids, such as sterols and/or HBI-trienes, which are indicative of open-water conditions (Belt and Müller, 2013; Lamping et al., 2020; Etourneau et al., 2013; Vorrath et al., 2019, 2020). The combination of the sea-ice biomarker and a phytoplankton biomarker, the so-called PIPSO₂₅ index (Vorrath et al., 2019), allows for a more quantitative differentiation of contrasting sea-ice settings and helps to avoid misinterpretations of the absence of IPSO₂₅. An absence of the sea-ice biomarker can result from either a lack of sea-ice cover or a permanent thick sea-ice cover that prevents light penetration and, hence, limits ice algae growth. These two contrasting scenarios can be distinguished by using the additional phytoplankton biomarker. Recently, Lamping et al. (2020) used the PIPSO₂₅ index to reconstruct changes in sea-ice conditions during the last deglaciation of the Amundsen Sea shelf, which were likely linked to advance and retreat phases of the Getz Ice Shelf.

Multiple mechanisms exist that can cause ice-shelf instability. As previously mentioned, relatively warm CDW is considered one of the main drivers for ice-shelf thinning in the Amundsen Sea and Bellingshausen Sea sectors of the West Antarctic Ice Sheet (Nakayama et al., 2018; Jenkins and Jacobs, 2008; Rignot et al., 2019). Accordingly, changing ocean temperatures are another crucial factor for the stability of the marine-based ice streams draining most of the West Antarctic Ice Sheet (e.g. Colleoni et al., 2018). As for sea-ice reconstructions, organic geochemical lipid proxies have been employed over the past decades to reconstruct ocean temperatures at high latitudes, as the abundance and preservation of calcareous microfossils commonly used for such reconstructions is very poor in polar marine sediments (e.g. Zamelczyk et al., 2012). In contrast, archaeal isoprenoidal glycerol dialkyl glycerol tetraethers (isoGDGTs), which are sensitive to temperature change and relatively resistant to degradation processes, are well preserved in all types of marine sediments (Huguet et al., 2008; Schouten et al., 2013). Schouten et al. (2002) found that the number of rings in sedimentary GDGTs is correlated with surface water temperatures, and they developed the first archaeal lipid palaeother-

momenter TEX_{86}^L , a ratio of certain GDGTs, as a sea surface temperature (SST) proxy. For polar oceans, Kim et al. (2010) developed a more specific calibration model for temperatures below 15 °C, TEX_{86}^L , which employs a different GDGT combination. There is an emerging consensus that GDGTs predominantly reflect subsurface ocean temperatures (SOT) along the Antarctic margin (Kim et al., 2012; Etourneau et al., 2019; Liu et al., 2020). This is supported by observations of elevated archaeal abundances (and GDGTs) in warmer subsurface waters (Liu et al., 2020; Spencer-Jones et al., 2021). Archaea adapt their membrane in cold waters by adding hydroxyl groups and changing the number of rings, OH-GDGTs (Fietz et al., 2020). Using molecular dynamic simulations, Huguet et al. (2017) found that the additional hydroxyl moieties lead to an increase in the membrane fluidity, which aids transmembrane transport in cold environments. This explains the higher relative abundance of OH Archaea lipids in cold environments. Taking the OH-GDGTs into account, Lü et al. (2015) proposed an SST proxy for the polar oceans, the RI-OH'.

The aim of our study is to provide insight into the application of biomarkers in Southern Ocean sediments as sea-ice and ocean temperature proxies. Estimates on recent sea-ice coverage and ocean temperatures along the eastern and western Antarctic Peninsula (EAP and WAP respectively) as well as in the Amundsen and Weddell seas are based on the analyses of IPSO₂₅, HBI-trienes and phytosterols, and GDGTs in seafloor surface sediment samples from these areas. A comparison of biomarker-derived estimates of sea-ice extent and ocean temperature with (1) sea-ice distributions obtained from satellite observations and (2) in situ ocean temperature measurements allows for an evaluation of the proxy approach. We further consider AWI-ESM2 climate model data to assess the model's performance in depicting recent oceanic key variables and to examine the potential impact of palaeoclimate conditions on the biomarker composition of the investigated surface sediments. Taking the various factors affecting the use of marine biomarkers as palaeoenvironmental proxies into account, we comment on the limitations of GDGT temperature estimates and the novel PIPSO₂₅ approach. Furthermore, we discuss the potential connection between IPSO₂₅ and platelet ice formation under near-coastal fast ice, which is related to the near-surface presence of sub-ice-shelf melt water.

2 Regional setting

The areas investigated in this study include the southern Drake Passage, the continental shelves of the WAP and EAP (~60° S), and the more southerly located Amundsen and Weddell seas (~75° S; Fig. 1). The different study areas are all connected by the Antarctic Circumpolar Current (ACC), the Antarctic Coastal Current and the Weddell Gyre respectively (Meredith et al., 2011; Rintoul et al., 2001).

The ACC, which is mainly composed of CDW and characterized by strong eastward flow, is the largest current system in the world and has its narrowest constriction in the Drake Passage. In the Amundsen Sea, the Bellingshausen Sea and along the WAP, where the ACC flows close to the continental shelf edge, CDW upwells onto the shelf and flows to the coast via bathymetric troughs, contributing to basal melt and retreat of marine-terminating glaciers and ice shelves (Cook et al., 2016; Jacobs et al., 2011; Jenkins and Jacobs, 2008; Klinck et al., 2004). In the Weddell Sea, the Weddell Gyre, a subpolar cyclonic circulation south of the ACC, deflects part of the CDW from the ACC towards the south and turns it into Warm Deep Water (WDW; Fig. 1; Hellmer et al., 2016; Vernet et al., 2019). In close vicinity to the Filchner–Ronne and Larsen ice shelves, glacial meltwater as well as dense brines released during sea-ice formation contribute to the formation of Weddell Sea Bottom Water (WSBW) – a major precursor of Antarctic Bottom Water (Hellmer et al., 2016). Along the EAP coast, wind and currents force a northward drift of sea ice (Harms et al., 2001), which melts when reaching warmer waters in the north and in Powell Basin (Vernet et al., 2019). At the northern tip of the Antarctic Peninsula, colder and saltier Weddell Sea water masses branch off westwards into the Bransfield Strait, where they encounter the well-stratified, warm and fresh Bellingshausen Sea Water (BSW; Fig. 1), which is entering the Bransfield Strait from the west (Sangrà et al., 2011).

Since 1978, satellite observations show strong seasonal and decadal changes in sea-ice cover around the Antarctic Peninsula, which are less pronounced in the Amundsen and Weddell seas (Vaughan et al., 2003; Parkinson and Cavalieri, 2012). Mean monthly sea-ice concentration (SIC) values for austral winter (JJA), spring (SON) and summer (DJF) reveal a permanently ice-free Drake Passage, whereas the WAP and EAP shelf areas are influenced by changing sea-ice cover throughout the year (Fig. 2a, b, c). For the Amundsen and Weddell seas, satellite data reveal up to ~90 % sea-ice concentration during winter and spring (Fig. 2a, b), and a minimum concentration of ~30 % during summer (Fig. 2c).

3 Material and methods

3.1 Sediment samples

We analysed a set of 41 surface sediment samples (0–1 cm sub-bottom depth) from different areas of the Southern Ocean (Fig. 1) retrieved by multicorers and giant box corers during RV *Polarstern* expeditions over the past 15 years. Sixteen surface sediment samples from the Amundsen Sea continental shelf were collected during expeditions PS69 in 2006 (Gohl, 2007) and PS104 in 2017 (Gohl, 2017). Twenty-five surface sediment samples from the southeastern and southwestern Weddell Sea continental shelf were collected during expeditions PS111 in 2018 (Schröder, 2018) and PS118 in 2019 (Dorschel, 2019). This new data set was complemented

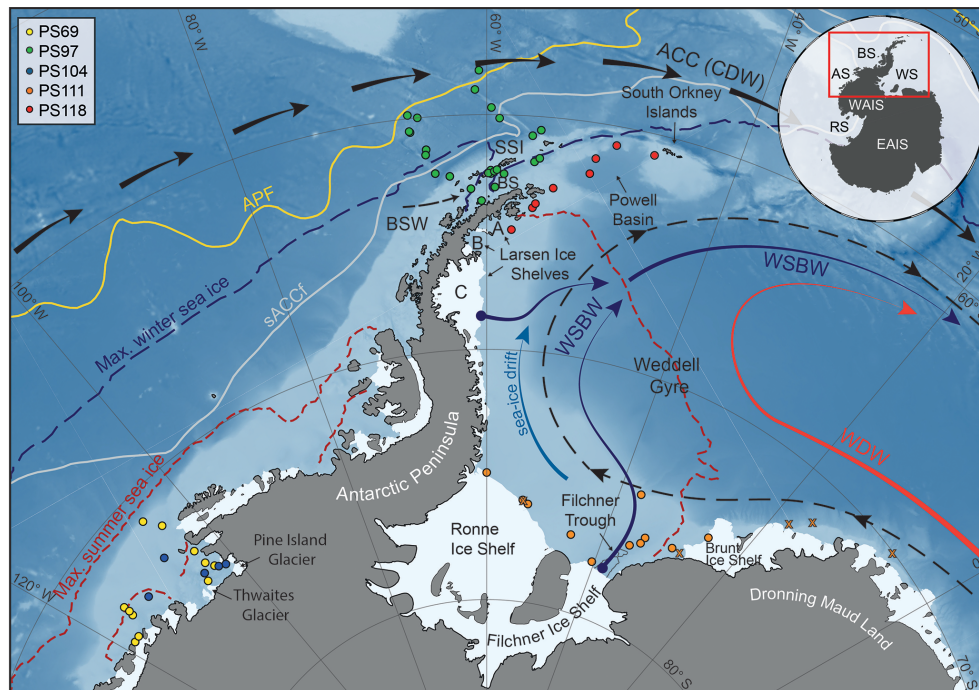


Figure 1. Map of the study area (location indicated by the red box in the inset) including all 41 sample locations (see different coloured dots for individual RV *Polarstern* expeditions in the top-left corner; for detailed sample information, see Table S1 in the Supplement) and the main oceanographic features. Maximum summer and winter sea-ice boundaries are marked by dashed red and blue lines respectively (Fetterer et al., 2016). The orange crosses in the Weddell Sea indicate samples with low biomarker concentrations close to the detection limit, to which we assigned a PIPSO₂₅ value of 1. The abbreviations use in the figure are as follows: ACC – Antarctic Circumpolar Current, APF – Antarctic Polar Front, sACCf – southern Antarctic Circumpolar Current Front, SSI – South Shetland Islands, BS – Bransfield Strait, BSW – Bellingshausen Sea Water, CDW – Circumpolar Deep Water, WDW – Weddell Deep Water and WSBW – Weddell Sea Bottom Water (Mathiot et al., 2011; Orsi et al., 1995). The inset shows grounded ice (i.e. without ice shelves) in black. The following abbreviations are used in the inset: WAIS – West Antarctic Ice Sheet, EAIS – East Antarctic Ice Sheet, RS – Ross Sea, AS – Amundsen Sea, BS – Bellingshausen Sea and WS – Weddell Sea. The background bathymetry is derived from International Bathymetric Chart of the Southern Ocean (IBCSO) data (Arndt et al., 2013).

by data from 26 surface sediment samples collected in Bransfield Strait/WAP, which were previously published by Vorath et al. (2019).

3.2 Bulk sediment and organic geochemical analyses

The sediment material was freeze-dried and homogenized with an agate mortar and stored in glass vials at -20°C before and after the above-mentioned initial preparation steps in order to avoid degradation of targeted molecular components. Total organic carbon (TOC) contents were measured on 0.1 g of sediment after removing inorganic carbon (total inorganic carbon, carbonates) with 500 μL 12 N hydrochloric acid. TOC contents were determined with a carbon–sulfur analyser (CS 2000; Eltra) with standards for calibration being routinely measured before sample analysis and after every 10th sample (error $\pm 0.02\%$).

Lipid biomarkers were extracted from the sediments (4 g for PS69 and PS104, and 6 g for PS111 and PS118) by ultrasonication (3×15 min) using DCM : MeOH (3×6 mL

for PS69 and PS104, and 3×8 mL for PS111 and PS118; 2 : 1 v/v) as solvent. Prior to this step, the internal standards 7-hexylnonadecane (7-HND; 0.038 μg per sample for PS69 and PS104, 0.057 μg per sample for PS111 and PS118), 5α -androstan-3-ol (1.04 μg per sample) and C₄₆ (0.98 μg per sample) were added to the sample for quantification of HBIs, sterols and GDGTs respectively. Via open-column chromatography, with SiO₂ as stationary phase, fractionation of the extract was achieved by eluting the apolar fraction (HBIs) and the polar fraction (sterols and GDGTs) with 5 mL *n*-hexane and 5 mL DCM : MeOH 1 : 1 respectively. The polar fraction was subsequently split into two fractions (sterols and GDGTs) for further processing. The sterol fraction was silylated with 300 μL bis-(trimethylsilyl)-trifluoroacetamide (BSTFA; 2 h at 60°C). Compound analyses of HBIs and sterols were carried out on an Agilent Technologies 7890B gas chromatograph (GC; fitted with a 30 m DB 1MS column; 0.25 mm diameter and 0.25 μm film thickness) coupled to an Agilent Technologies 5977B mass selective detector (MSD; with 70 eV constant ionization potential, ion source temper-

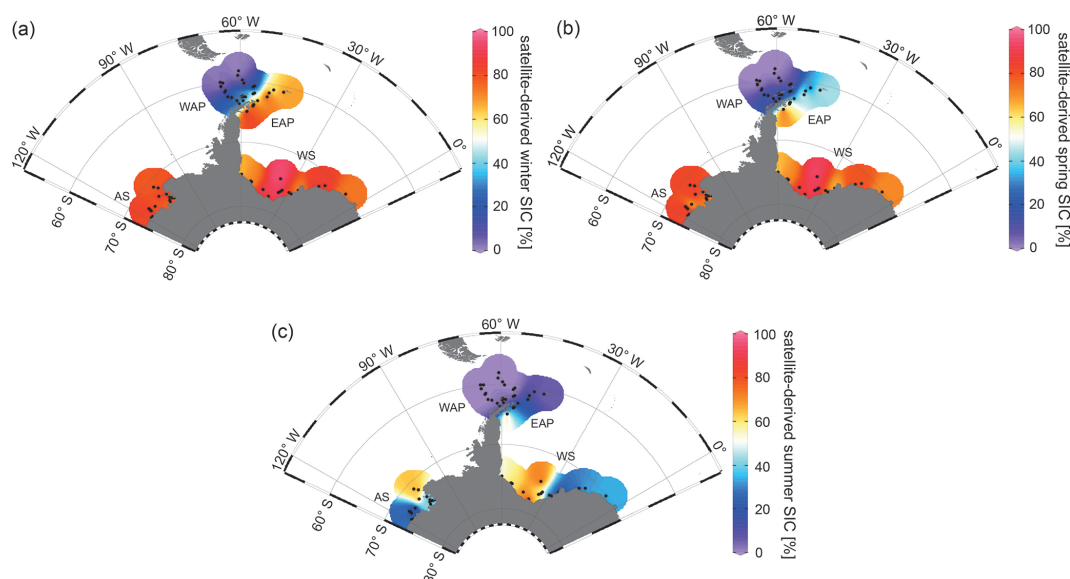


Figure 2. Distribution of mean monthly satellite-derived sea-ice concentration (SIC) for (a) winter (JJA), (b) spring (SON) and (c) summer (DJF) in percent (downloaded from the National Snow and Ice Data Center, NSIDC; Cavalieri et al., 1996). The following abbreviations are used in the figure: AS – Amundsen Sea, WAP – West Antarctic Peninsula, EAP – East Antarctic Peninsula and WS – Weddell Sea. Maps were generated using the Ocean Data View Software (ODV; Schlitzer, 2017).

ature of 230 °C). The GC oven was set to 60 °C (3 min), 150 °C (rate: 15 °C min⁻¹), 320 °C (rate: 10 °C min⁻¹) and 320 °C (15 min isothermal) for the analysis of hydrocarbons and to 60 °C (2 min), 150 °C (rate: 15 °C min⁻¹), 320 °C (rate: 3 °C min⁻¹) and 320 °C (20 min isothermal) for the analysis of sterols. Helium was used as the carrier gas. The HBI and sterol compounds were identified by their GC retention times and mass spectra (Belt et al., 2018, 2000; Boon et al., 1979). Lipids were quantified by setting the individual, manually integrated, gas chromatograph–mass spectrometer peak area in relation to the peak area of the respective internal standard and normalization to the amount of extracted sediment. IPSO₂₅ and HBI-trienes were quantified by relating their molecular ions (IPSO₂₅, *m/z* 348, and HBI-trienes, *m/z* 346) to the fragment ion *m/z* 266 of the internal standard 7-HND (Belt, 2018). Sterols were quantified by comparing the molecular ion of the individual sterol with the molecular ion *m/z* 348 of the internal standard 5 α -androstan-3-ol. Instrumental response factors for the target lipids were considered as recommended by Belt et al. (2014) and Fahl and Stein (2012). All biomarker concentrations were subsequently normalized to the TOC content of each sample to account for different depositional settings within the different study areas.

For calculating the phytoplankton IPSO₂₅ (PIPSO₂₅) index, we used the equation introduced by Vorrath et al. (2019):

$$\text{PIPSO}_{25} = \text{IPSO}_{25} / (\text{IPSO}_{25} + (\text{phytoplankton marker} \times c)), \quad (1)$$

where *c* (*c* = mean IPSO₂₅/mean phytoplankton marker) is applied as a concentration balance factor to account for high

concentration offsets between IPSO₂₅ and the phytoplankton biomarker (see Table 1 in the Supplement for *c* factors of individual PIPSO₂₅ calculations).

Following the approach by Müller and Stein (2014) and Lamping et al. (2020), a PIPSO₂₅ value of 1 was assigned to samples with exceptionally low (at the detection limit) concentrations of both biomarkers (see chap. 4.1.2). This comprises the five Weddell Sea samples PS111/13-2, /15-1, /16-3, /29-3 and /40-2 (marked as an orange x in Fig. 1).

The GDGT fraction was dried under N₂, redissolved with 120 μ L hexane : isopropanol (*v/v* 99 : 1) and then filtered using a polytetrafluoroethylene (PTFE) filter with a 0.45 μ m pore size membrane. GDGTs were measured using a high-performance liquid chromatograph (HPLC; Agilent 1200 series HPLC system) coupled to an Agilent 6120 mass spectrometer (MS), operating with atmospheric pressure chemical ionization (APCI). The injection volume was 20 μ L. For separating the GDGTs, a Prevail Cyano 3 μ m column (Grace, 150 mm \times 2.1 mm) was kept at 30 °C. Each sample was eluted isocratically for 5 min with solvent A (hexane/2-propanol/chloroform; 98 : 1 : 1) at a flow rate of 0.2 mL min⁻¹, and the volume of solvent B (hexane/2-propanol/chloroform; 89 : 10 : 1) was increased linearly to 10 % within 20 min and then to 100 % within 10 min. The column was back-flushed (5 min, flow rate of 0.6 mL min⁻¹) after 7 min and after each sample and was re-equilibrated with solvent A (10 min, flow rate of 0.2 mL min⁻¹). The APCI was set to the following: N₂ drying gas flow at 5 L min⁻¹ and temperature to 350 °C, nebulizer pressure to 50 psi, vaporizer gas temperature to 350 °C, capillary volt-

age to 4 kV and corona current to +5 μ A. Detection of GDGTs was achieved by means of selective ion monitoring (SIM) of $[M+H]^+$ ions (dwell time 76 ms). GDGT-0 (m/z 1302), GDGT-1 (m/z 1300), GDGT-2 (m/z 1298), GDGT-3 (m/z 1296) and crenarchaeol (m/z 1292) as well as brGDGT-III (m/z 1050), brGDGT-II (m/z 1036) and brGDGT-I (m/z 1022) were quantified by relating their molecular ions to the molecular ion m/z 744 of the internal standard C_{46} -GDGT. The late eluting hydroxylated GDGTs (OH-GDGT-0, OH-GDGT-1 and OH-GDGT-2 with m/z 1318, 1316 and 1314 respectively) were quantified in the scans (m/z 1300, 1298 and 1296) of their related GDGTs, as described by Fietz et al. (2013).

TEX_{86}^L values and their conversion into SOTs were determined following Kim et al. (2012):

$$TEX_{86}^L = \text{LOG} \frac{[\text{GDGT} - 2]}{[\text{GDGT} - 1] + [\text{GDGT} - 2] + [\text{GDGT} - 3]}, \quad (2)$$

$$\text{SOT}^{\text{TEX}} [^\circ\text{C}] = 50.8 \times \text{TEX}_{86}^L + 36.1. \quad (3)$$

Temperature calculations based on OH-GDGTs were carried out according to Lü et al. (2015):

$$\text{RI-OH}' = \frac{[\text{OH} - \text{GDGT} - 1] + 2 \times [\text{OH} - \text{GDGT} - 2]}{[\text{OH} - \text{GDGT} - 0] + [\text{OH} - \text{GDGT} - 1] + [\text{OH} - \text{GDGT} - 2]}, \quad (4)$$

$$\text{SST}^{\text{OH}} [^\circ\text{C}] = \text{RI} - \text{OH}' - 0.1/0.0382. \quad (5)$$

To determine the relative influence of terrestrial organic matter input, the branched isoprenoid tetraether (BIT) index was calculated following Hopmans et al. (2004):

$$\text{BIT} = \frac{[\text{brGDGT} - \text{I}] + [\text{brGDGT} - \text{II}] + [\text{brGDGT} - \text{III}]}{[\text{Chrenarchaeol}] + [\text{brGDGT} - \text{I}] + [\text{brGDGT} - \text{II}] + [\text{brGDGT} - \text{III}]}. \quad (6)$$

3.3 Numerical model

3.3.1 Model description

AWI-ESM2 is a state-of-the-art coupled climate model developed by Sidorenko et al. (2019) which comprises an atmospheric component ECHAM6 (Stevens et al., 2013) as well as an ocean–sea-ice component FESOM2 (Danilov et al., 2017). The atmospheric module ECHAM6 is the most recent version of the ECHAM model developed at the Max Planck Institute for Meteorology (MPI) in Hamburg. The model is branched from an early release of the European Center (EC) for Medium-Range Weather Forecasts (ECMWF) model (Roeckner et al., 1989). ECHAM6 dynamics is based on hydrostatic primitive equations with traditional approximation. We used a T63 Gaussian grid with a spatial resolution of about $1.9^\circ \times 1.9^\circ$ (1.9° or 210 km). There are 47 vertical layers in the atmosphere.

Momentum transport arising from boundary effects is configured using the sub-grid orography scheme as described by Lott (1999). Radiative transfer in ECHAM6 is represented

by the method described in Iacono et al. (2008). ECHAM6 also contains a land surface model (JSBACH) which includes 12 plant functional types of dynamic vegetation and 2 bare-surface types (Loveland et al., 2000; Raddatz et al., 2007). The ice–ocean module in AWI-ESM2 is based on the finite volume discretization formulated on unstructured meshes. The multi-resolution for the ocean is up to 15 km over polar and coastal regions, and 135 km for far-field oceans, with 46 uneven vertical depths. The impact of local dynamics on the global ocean is related to a number of FESOM-based studies (Danilov et al., 2017). The multi-resolution approach advocated by FESOM allows one to explore the impact of local processes on the global ocean with moderate computational effort (Danilov et al., 2017). AWI-ESM2 employs the OASIS3-MCT coupler (Valcke, 2013) with an intermediate regular exchange grid. Mapping between the intermediate grid and the atmospheric/oceanic grid is handled with bilinear interpolation. The atmosphere component computes 12 air–sea fluxes based on four surface fields provided by the ocean module FESOM2. AWI-ESM2 has been validated under modern climate conditions (Sidorenko et al., 2019) and has been applied for marine radiocarbon concentrations (Lohmann et al., 2020), the latest Holocene (Vorrath et al., 2020), and the Last Interglacial (Otto-Bliesner et al., 2021).

3.3.2 Experimental design

One transient experiment was conducted using AWI-ESM2, which applied the boundary conditions, including orbital parameters and greenhouse gases. Orbital parameters are calculated according to Berger (1978), and the concentrations of greenhouse gases are taken from ice-core records and measurements of recent firn air and atmospheric samples (Köhler et al., 2017). The model was initialized from a 1000-year spin-up run under mid-Holocene (6000 BP, before present) boundary conditions as described by Otto-Bliesner et al. (2017). In our modelling strategy, we follow Lorenz and Lohmann (2004) and use the climate condition from the mid-Holocene spin-up run as the initial state for the subsequent transient simulation covering the period from 6000 BP to 2014 CE (Common Era). In the present study, we derived seasonal SIC, SSTs and SOTs in the study areas from a segment of the transient experiment (1950–2014 CE). Topography including prescribed ice-sheet configuration was kept constant in our transient simulation. All model data are provided in Table S2 in the Supplement.

3.4 Satellite SIC and SSTs

Satellite sea-ice data were derived from Nimbus-7 Scanning Multichannel Microwave Radiometer (SMMR) and Defence Meteorological Satellite Program (DMSP) Special Sensor Microwave Imager/Sounder (SSM/I-SSMIS) passive microwave data and downloaded from the National Snow and Ice Data Center (NSIDC; Cavalieri et al., 1996). The

sea-ice data represent mean monthly SIC values, which are expressed to range from 0% to 100% and are averaged over a period from the beginning of satellite observations in 1978 CE to the individual year of sample collection. The monthly mean SIC values were then split into different seasons: winter (JJA), spring (SON) and summer (DJF) (Fig. 2a, b, c), and these data are considered to represent the recent mean state of sea-ice coverage. All satellite data are provided in Table S3.

Modern annual mean SSTs and SOTs were derived from the World Ocean Atlas 2013 and represent averaged values for the years 1955–2012 CE (WOA13; Locarnini et al., 2013).

4 Results and discussion

In the following, we first present and discuss the biomarker data generated for this study from north (Antarctic Peninsula) to south (Amundsen and Weddell seas) and draw conclusions about the environmental settings deduced from the data set. In regard to the phytoplankton-derived biomarkers, we focus on the significance of HBI Z-triene and brassicasterol, because the HBI E-triene and dinosterol data, which are presented in the Supplement (Fig. S1), show very similar patterns. All data are provided in Table S1 and are available from the PANGAEA data repository (<https://doi.org/10.1594/PANGAEA.932265>). For the discussion of the target environmental variables, i.e. PIPSO₂₅-based sea-ice and GDGT-derived ocean temperature estimates, satellite, instrumental and model data are considered. In Sect. 5, we further address potential caveats in biomarker-based environmental reconstructions that need to be taken into account when applying these proxies.

4.1 TOC content, HBIs and sterols in Antarctic surface sediments

TOC contents in marine sediments are often viewed as an indicator for primary productivity in surface waters (Meyers, 1997). However, we are aware that additional factors, such as different water depths and depositional regimes, may exert control on sedimentary TOC as well. The TOC contents of the investigated surface samples are lowest in Drake Passage with values of around 0.12%–0.54% and increase from northwest to southeast into Bransfield Strait, where they range from 0.59% to 1.06% (WAP, Fig. 3a). Along the EAP, higher TOC contents (0.57%–0.86%) prevail around the former Larsen A Ice Shelf and north of James Ross Island, but they decrease towards Powell Basin (0.22%–0.37%) and then increase to 0.50% around the South Orkney Islands, which may point to elevated productivity or an enhanced supply of reworked terrigenous organic matter in this area (EAP, Fig. 3a).

At the WAP, concentrations of the sea-ice biomarker IP_{SO}₂₅ increase from northwest to southeast. IP_{SO}₂₅ is absent in samples from the permanently ice-free Drake Passage and increases towards the continental slope and the seasonally ice-covered shelf (0.37–17.81 μg g OC⁻¹; Fig. 3b; Vorrath et al., 2019). The highest IP_{SO}₂₅ concentrations are observed in samples of the northern Bransfield Strait. Here, the inflow of waters from the Weddell Sea transports sea ice into Bransfield Strait (Vorrath et al., 2019). Elevated IP_{SO}₂₅ concentrations are also observed at the seasonally sea-ice-covered EAP, where relatively high concentrations of the sea-ice biomarker prevail in samples located in the area of the former Larsen A Ice Shelf and north of James Ross Island (12.59–17.74 μg g OC⁻¹; Fig. 3b). Because these locations are influenced by the northward drift of sea ice within the Weddell Gyre (Fig. 1), the elevated IP_{SO}₂₅ concentrations could also result from sea ice advected from the southern Weddell Sea. We suggest that the decrease in IP_{SO}₂₅ concentrations towards the Powell Basin and the South Orkney Islands (0.59–5.36 μg g OC⁻¹; Fig. 3b) is connected to warmer ocean temperatures in the north and reduced sea-ice cover during spring.

Concentrations of the phytoplankton biomarker HBI Z-triene around the Antarctic Peninsula are highest in eastern Drake Passage and along the WAP continental slope (where IP_{SO}₂₅ is absent) and decrease in Bransfield Strait (0.33–26.86 μg g OC⁻¹; Fig. 3c; Vorrath et al., 2019). Elevated HBI Z-triene concentrations have, so far, been detected in surface waters along the sea-ice edge (Smik et al., 2016) and, hence, were suggested to be a proxy for marginal ice zone conditions (Belt et al., 2015; Collins et al., 2013; Schmidt et al., 2018). Vorrath et al. (2019), however, relate the high concentrations of HBI Z-triene at the northernmost stations in the permanently ice-free eastern Drake Passage to their proximity to the Antarctic Polar Front. Here, productivity of the source diatoms of HBI-trienes (e.g. *Rhizosolenia* spp.; Belt et al., 2017) may be enhanced by meander-induced upwelling leading to increased nutrient flux to surface waters (Moore and Abbott, 2002). As Cárdenas et al. (2019) document only minor abundances of *Rhizosolenia* spp. in seafloor surface sediments from this area, we assume that HBI-trienes might also be biosynthesized by other diatom taxa. Moderate concentrations along the continental slope of the WAP and in Bransfield Strait were associated with elevated inflow of warm BSW which leads to a retreating sea-ice margin during spring and summer (for more details, see Vorrath et al., 2019, 2020). Samples from the EAP shelf and Powell Basin are characterized by relatively low HBI Z-triene concentrations (0.1–2.37 μg g OC⁻¹; Fig. 3c) that decrease from southwest to northeast, whereas the northernmost sample closest to the South Orkney Islands is characterized by an elevated HBI Z-triene concentration of ~8.49 μg g OC⁻¹ (EAP, Fig. 3c). This relatively high concentration may be related to an “island mass effect”, coined by Doty and Oguri (1956), which refers to increased primary production around oceanic

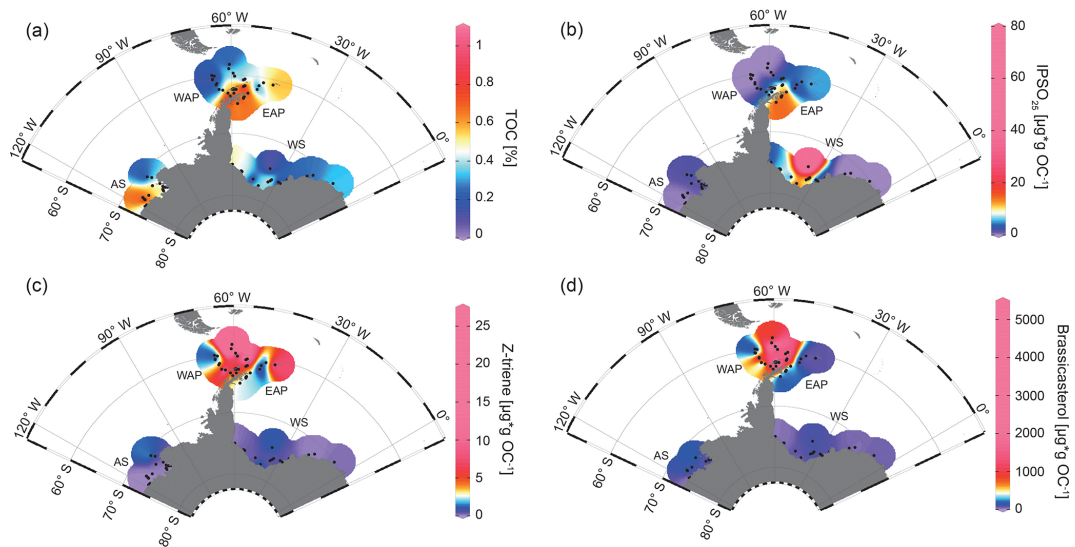


Figure 3. Distribution of (a) TOC (%), (b) IPSO₂₅, (c) HBI Z-triene and (d) brassicasterol in surface sediment samples. Sample locations are marked as black dots. Concentrations of biomarkers ($\mu\text{g g OC}^{-1}$) were normalized to the TOC content of each sample. The abbreviations used in the figure are as follows: AS – Amundsen Sea, WAP – West Antarctic Peninsula, EAP – East Antarctic Peninsula and WS – Weddell Sea. Maps were generated using the Ocean Data View Software (Schlitzer, 2017).

islands in comparison to surrounding waters. Nolting et al. (1991) found extraordinarily high dissolved iron levels (as high as 50–60 nM) on the South Orkney shelf, while Nielsdóttir et al. (2012) observed enhanced iron and Chl-*a* concentrations in the vicinity of the South Orkney Islands. These authors explain the increased dissolved iron levels with input from seasonally retreating sea ice, which is recorded by satellites (Fig. 2a, b, c) and probably leads to substantial annual phytoplankton blooms, which may also cause the elevated TOC content in the corresponding seafloor sediment sample (Fig. 3a). Alternatively, remobilization of shelf sediments or vertical mixing of iron-rich deep waters, leading to high iron contents in surface waters, may stimulate primary productivity (Blain et al., 2007; de Jong et al., 2012). However, it remains unclear why the brassicasterol concentration is distinctly low in this sample, and we assume that different environmental preferences of the source organisms may account for this. In Drake Passage and along the EAP, brassicasterol displays a similar pattern to HBI Z-triene, with relatively high concentrations (more than 2 orders of magnitudes) ranging from 1.86 to 5017.44 $\mu\text{g g OC}^{-1}$ (Fig. 3d).

In the Weddell Sea, TOC contents are generally low (<0.4%), with slightly elevated values in the west (up to 0.50%) and right in front of the Filchner Ice Shelf (up to 0.52%; Fig. 3a). The Amundsen Sea is characterized by slightly higher TOC contents, with concentrations of up to 0.91% in the west and lower values in the east (0.33%; AS, Fig. 3a).

In the samples from the Amundsen and Weddell seas, which are both dominated by strong winter sea-ice cover lasting until spring (Fig. 2a, b, c), all three biomarkers

are present in low concentrations only. An exception are the samples located in front of the Filchner Ice Shelf with significantly higher concentrations of IPSO₂₅ (7.09–73.87 $\mu\text{g g OC}^{-1}$; WS, Fig. 3b). Concentrations of IPSO₂₅ on the Amundsen Sea shelf are relatively low (0.04–3.3 $\mu\text{g g OC}^{-1}$), with slightly higher values observed in the northeast (AS, Fig. 3b). HBI Z-triene concentrations are also very low but are slightly higher in Filchner Trough (0.04–1 $\mu\text{g g OC}^{-1}$) and at more distal locations on the northeastern Amundsen Sea shelf (0.01–1.88 $\mu\text{g g OC}^{-1}$; Fig. 3c). Brassicasterol generally shows a similar pattern to HBI Z-triene, with concentrations varying between 1.86 and 220.54 $\mu\text{g g OC}^{-1}$ (Fig. 3d; for HBI E-triene and dinosterol distribution, see Fig. S1).

4.2 Combining individual biomarker records: the PIPSO₂₅ index

The PIPSO₂₅ index combines the relative concentrations of IPSO₂₅ and a selected phytoplankton biomarker, such as HBI-trienes and sterols, as an indicator for an open-ocean environment (Vorrath et al., 2019). The combination of both endmembers (sea ice vs. open ocean) prevents misleading interpretations regarding the absence of IPSO₂₅ in the sediments, which can be the result of two entirely different scenarios. Under heavy/perennial sea-ice coverage, the thickness of sea ice hinders light penetration, thereby limiting the productivity of algae living in basal sea ice (Hancke et al., 2018). This scenario can cause the absence of both phytoplankton and sea-ice biomarkers in the sediment. The other scenario depicts a permanently open ocean, where the sea-

ice biomarker is absent as well, but here the phytoplankton biomarkers are present in variable concentrations (Müller et al., 2011). The presence of both biomarkers in the sediment is indicative of seasonal sea-ice coverage and/or the occurrence of stable sea-ice margin conditions, promoting biosynthesis of both biomarkers (Müller et al., 2011). Here, we distinguish between P_Z IPSO₂₅ and P_B IPSO₂₅ using HBI Z-triene and brassicasterol as a phytoplankton biomarker respectively (Fig. 4a, b; for PIPSO₂₅ values based on HBI E-triene and dinosterol, see Table S1 and Fig. S2).

Both PIPSO₂₅ indices are 0 in the predominantly ice-free Drake Passage and increase towards southeast to intermediate values on the WAP slope and around the South Shetland Islands, reflecting increased influence of marginal sea-ice cover towards the coast (0.02–0.70; Vorrath et al., 2019). At the seasonally sea-ice-covered EAP, P_Z IPSO₂₅ values reach 0.84, while lower values of around 0.25 are observed close to the South Orkney Islands, which is caused by the elevated HBI Z-triene concentrations at the stations there (EAP, Fig. 3c). The P_B IPSO₂₅ index exhibits even higher values of up to 0.98 at the EAP/northwestern Weddell Sea. These elevated PIPSO₂₅ indices align well with the significant northward sea-ice drift within the Weddell Gyre, which leads to prolonged sea-ice cover along the EAP.

In samples from the southern Weddell Sea, both PIPSO₂₅ indices show a similar pattern with high values of up to 0.9, and slightly lower values are observed in front of the Brunt Ice Shelf (0.6; Fig. 4a, b). Very low concentrations (close to the detection limit) of both biomarkers in samples from the continental shelf off Dronning Maud Land (Fig. 1) result in low PIPSO₂₅ values, strongly underestimating the sea-ice cover in this area, where satellite-derived sea-ice data document severe seasonal sea-ice cover (Fig. 2). As previously mentioned, we followed the approach by Müller and Stein (2014) and Lamping et al. (2020) by assigning a maximum PIPSO₂₅ value of 1 to these samples to circumvent misleading interpretations and to aid visualization.

The intermediate PIPSO₂₅ value (~ 0.51) derived for one sample collected in front of the Brunt Ice Shelf points to less severe sea-ice cover in that area. A possible explanation for the relatively low PIPSO₂₅ value is the presence of a coastal polynya that has been reported by Anderson (1993) and which is further supported by Paul et al. (2015). These authors note that the sea-ice area around the Brunt Ice Shelf is the most active in the southern Weddell Sea, with an annual average polynya area of 3516 ± 1420 km². Interestingly, the reduced SIC here is also captured by our model (see Sect. 4.3).

PIPSO₂₅ values in the Amundsen Sea point to different scenarios. The P_Z IPSO₂₅ index varies around 0.9, with only the easterly, more distal samples having lower values between 0.3 and 0.6 (Fig. 4a). The P_B IPSO₂₅ index generally has lower values, ranging from 0.6 in the coastal area to 0.2 in the more distal samples (Fig. 4b). This difference between P_Z IPSO₂₅ and P_B IPSO₂₅ may be explained by the different

source organisms biosynthesizing the individual phytoplankton biomarkers. While the main origin of HBI-trienes seems to be restricted to diatoms (Belt et al., 2017), brassicasterol is known to be produced by several algal groups that are adapted to a wider range of sea surface conditions (Volkman, 2006; see Sect. 5.2).

4.3 Biomarker-based sea-ice estimates vs. satellite and model data

The main ice algae bloom in the Southern Ocean occurs during spring, when solar insolation and air temperatures/SSTs increase and sea ice starts to melt, which results in the release of nutrients and stratification of the water column, stimulating the productivity of photosynthesizing organisms (Arrigo, 2017; Belt, 2018). Hence, the sea-ice biomarker IPSO₂₅ is commonly interpreted as a spring sea-ice indicator, which is why, in the following, we compare the biomarker-based sea-ice reconstructions to satellite-derived and modelled spring SIC. IPSO₂₅ concentrations in the surface sediments around the Antarctic Peninsula exhibit similar trends to the satellite-derived and modelled SIC (Figs. 3, 4), whereas they differ significantly in the Amundsen and Weddell seas, where high SIC values are recorded by satellites and the model but IPSO₂₅ is present in low concentrations. The low IPSO₂₅ concentrations in these areas highlight the uncertainty, when considering IPSO₂₅ as a sea-ice proxy alone, as such low concentrations are not only observed under open-water conditions, but also under severe sea-ice cover. In the Amundsen and Weddell seas, the low IPSO₂₅ concentrations are the result of the latter, where limited light availability hinders ice algae growth, leading to an underestimation of sea-ice cover. Accordingly, we note a weak correlation between IPSO₂₅ data and satellite SIC ($R^2 = 0.19$; Fig. 5a). As stated above, the combination of IPSO₂₅ and a phytoplankton marker may prevent this ambiguity. The higher sea-ice concentrations in the Amundsen and Weddell seas are better reflected by maximum P_Z IPSO₂₅ values than by IPSO₂₅ alone. However, we note that the P_Z IPSO₂₅ index apparently does not resolve SIC values higher than 50 % (see Fig. S3), which may indicate a threshold (here ~ 50 % SIC) where the growth of the HBI-triene- and IPSO₂₅-producing algae is limited.

In general, however, the P_Z IPSO₂₅ values correlate much better with satellite and modelled SIC ($R^2 = 0.78$ and $R^2 = 0.76$ respectively; Fig. 5b, d) than IPSO₂₅ concentrations. Correlations of satellite and model data with PIPSO₂₅ calculated using HBI E-triene, brassicasterol and dinosterol respectively, are also positive but less significant (Fig. S4); hence, we focus the discussion on P_Z IPSO₂₅. The AWI-ESM2-derived spring SIC values correctly display the permanently ice-free Drake Passage and the northwest–southeast increase in sea-ice cover from the WAP continental slope towards Bransfield Strait (Fig. 4d). The model, however, significantly underestimates the elevated sea-ice concentrations (up to 70 %) in front of the former Larsen Ice

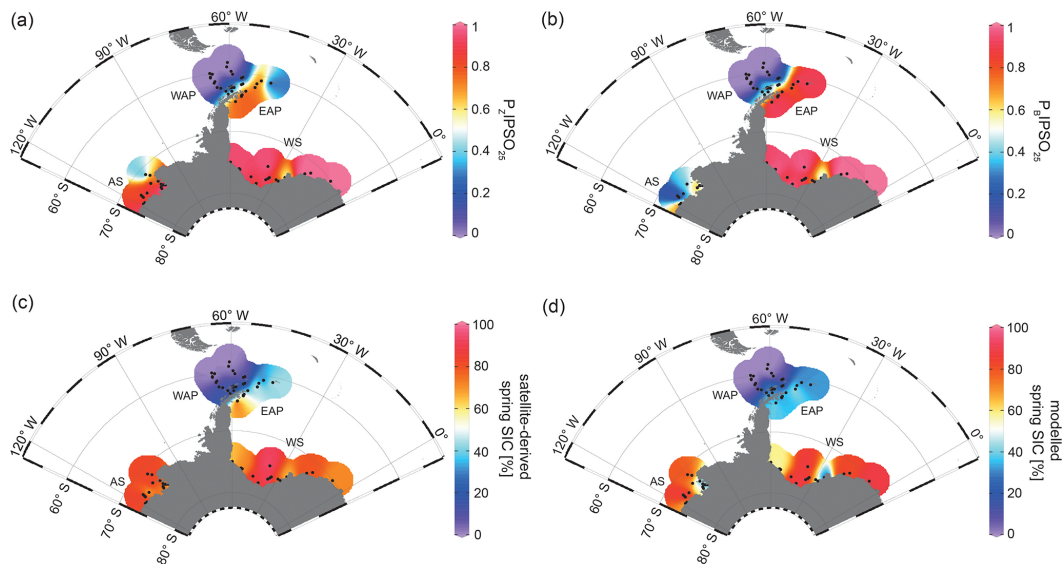


Figure 4. Distribution of the sea-ice index PIPSO₂₅ in surface sediment samples, with (a) P_ZIPSO₂₅ based on HBI Z-triene and (b) P_BIPSO₂₅ based on brassicasterol, (c) satellite-derived spring SIC (%) and (d) modelled spring SIC (%). The abbreviations used in the figure are as follows: AS – Amundsen Sea, WAP – West Antarctic Peninsula, EAP – East Antarctic Peninsula and WS – Weddell Sea. Maps were generated using the Ocean Data View Software (Schlitzer, 2017).

Shelf A and east of James Ross Island at the EAP observed in satellite data. In the Amundsen and Weddell seas, the model predicts heavy sea-ice cover ($\sim 90\%$), only slightly underestimating the sea-ice cover at the near-coastal sites in front of Pine Island Glacier and Ronne Ice Shelf. Interestingly, modelled SIC in front of Brunt Ice Shelf is as low as $\sim 45\%$ (Fig. 4d, e), corresponding well to the reduced P_ZIPSO₂₅ value of ~ 0.51 . This may reflect the polynya conditions in that region documented by Anderson (1993) and Paul et al. (2015). Overall, we note that modelled modern SIC values correlate well with satellite data ($R^2 = 0.73$; Fig. 5c) and P_ZIPSO₂₅ values ($R^2 = 0.76$; Fig. 5d), whereas we observe weaker correlations between modelled palaeo-SIC values and P_ZIPSO₂₅ values (Fig. S5; see Sect. 5.1).

4.4 TEX₈₆^L - and RI-OH'-derived ocean temperatures

For a critical appraisal of the applicability and reliability of GDGT indices as temperature proxies at polar latitudes, we here focus on the TEX₈₆^L proxy by Kim et al. (2012), which potentially reflects SOTs, and the RI-OH' proxy by Lü et al. (2015), which is assumed to reflect SSTs. The reconstructions are believed to represent annual mean ocean temperatures (for correlations of TEX₈₆^L-derived SOTs with WOA spring and winter SOTs, see Fig. S6). In all samples, the BIT index (Eq. 6) is < 0.3 , indicating no significant impact of terrestrial input of organic material on the distribution of GDGTs and, hence, their reliability as temperature proxy. RI-OH'-derived temperatures and TEX₈₆^L-derived SOTs both show a similar pattern, but different temperature ranges be-

tween -2.62 to $+4.67^\circ\text{C}$ and -2.38 to $+8.75^\circ\text{C}$ respectively (Fig. 6a, b). At the WAP, RI-OH'- and TEX₈₆^L-derived temperatures increase northwestwards across the Antarctic continental slope and into the permanently ice-free Drake Passage, which are influenced by the ACC and relatively warm CDW (Orsi et al., 1995; Rintoul et al., 2001). Temperatures decrease towards Bransfield Strait and the EAP, which are influenced by seasonal sea-ice cover and relatively cold water from the Weddell Sea that branches off the Weddell Gyre (Collares et al., 2018; Thompson et al., 2009). At the EAP, a southwestward decrease is observed, with relatively low temperatures at the former Larsen A Ice Shelf and higher temperatures recorded in Powell Basin and around the South Orkney Islands (Fig. 6a, b).

In the Amundsen and Weddell seas further south, reconstructed temperatures are generally lower than around the Antarctic Peninsula. Samples from the Weddell Sea display a temperature decrease from east to west, which may reflect the route of eddies in the northeastern Weddell Gyre. These eddies carry relatively warm, salty CDW westward along the southern limb of the Weddell Gyre, where it becomes WDW (Vernet et al., 2019). The coldest TEX₈₆^L and RI-OH' temperatures ($< 0^\circ\text{C}$) at sites along the Filchner–Ronne Ice Shelf front may be further linked to the presence of cold precursor water masses for WSBW.

With respect to ongoing discussions regarding whether GDGT-based temperature reconstructions represent SSTs or SOTs (Kalanetra et al., 2009; Kim et al., 2012; Park et al., 2019), we compare our RI-OH' and TEX₈₆^L-derived temperatures with surface and subsurface temperature data obtained

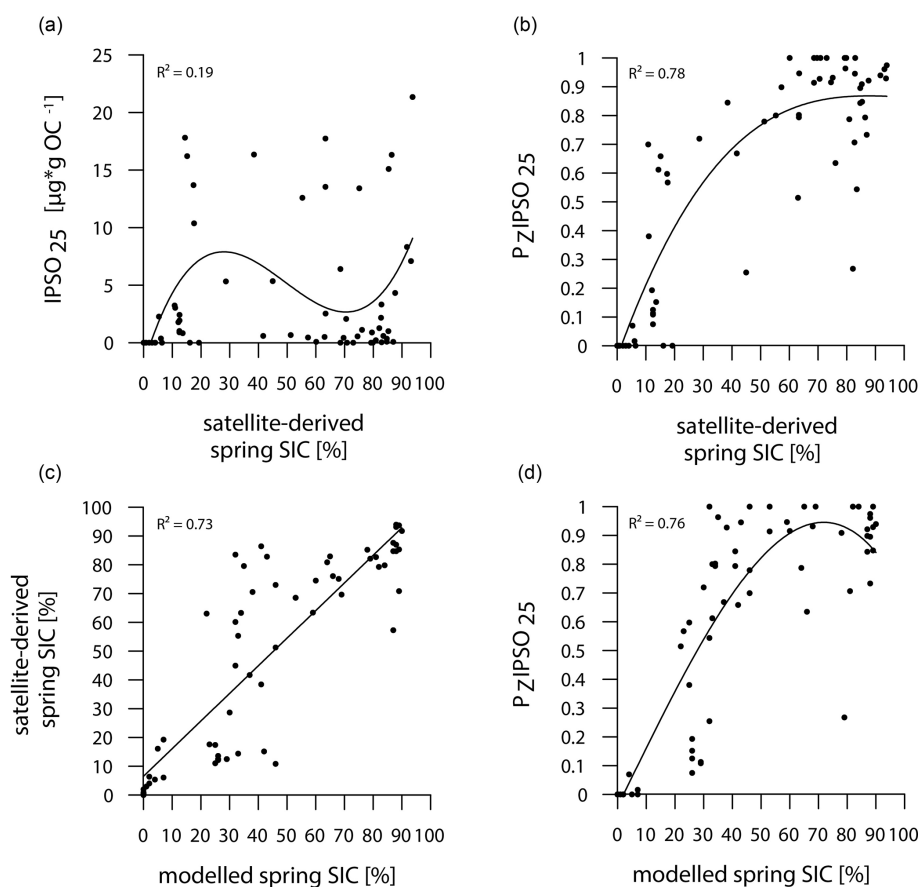


Figure 5. Correlations of (a) IPSO₂₅ concentrations vs. satellite-derived spring SIC, (b) PzIPSO₂₅ values vs. satellite-derived spring SIC, (c) satellite-derived spring SIC vs. modelled spring SIC and (d) PzIPSO₂₅ values vs. modelled spring SIC. Coefficients of determination (R^2) are given for the respective regression lines.

by in situ measurements and modelling (Fig. 6c, d, e, f). Comparison of GDGT-derived temperatures with WOA13 temperatures from different water depths reveals the most significant correlation for a water depth of 410 m (for respective correlations, see Fig. S7). Hence, when discussing instrumental and modelled SOTs, we refer to 410 m water depth.

While the correlation between TEX₈₆^L-derived SOTs and instrumental SOTs is reasonably good ($R^2 = 0.66$; Fig. 7a), also supporting a subsurface origin for the TEX₈₆^L proxy, we note a significant overestimation of SOTs by up to 6 °C in Drake Passage (Fig. S8). This warm-biased TEX₈₆^L signal is a known caveat and is, among others, assumed to be connected to GDGTs produced by deep-dwelling Euryarchaeota (Park et al., 2019), which have been reported in CDW (Alonso-Sáez et al., 2011) and in deep waters at the Antarctic Polar Front (López-García et al., 2001). Maximum TEX₈₆^L-based SOTs of 5–8 °C in the central Drake Passage (Fig. 6b), however, distinctly exceed the common temperature range of CDW (0–2 °C). Interestingly, TEX₈₆^L-derived SOTs in the colder regions of the Amundsen and Weddell seas relate reasonably well to instrumental temperatures and are only

slightly warm-biased (Fig. S8). Correlations between RI-OH'-derived temperatures and instrumental SSTs are weak ($R^2 = 0.43$; Fig. 7b). Recently, in their study on surface sediments from Prydz Bay (East Antarctica), Liu et al. (2020) concluded that the RI-OH' index also holds promise as a tool to reconstruct SOTs rather than SSTs. When correlating our RI-OH'-derived temperatures with instrumental SOTs, we similarly find a high correlation ($R^2 = 0.73$; Fig. 7c), supporting the above-mentioned hypothesis. We further note that the RI-OH' temperature range is much more realistic than the TEX₈₆^L range. This suggests that the addition of OH-isoGDGTs in the temperature index is a promising step towards reliable high-latitude temperature reconstructions and may improve our understanding of the temperature responses of archaeal membranes in Southern Ocean waters (Fietz et al., 2020; Park et al., 2019). Clearly, more data – ideally obtained from sediment traps, seafloor surface sediment samples and longer sediment cores – and calibration studies will help to further elucidate the applicability of the RI-OH' and TEX₈₆^L temperature reconstructions.

Similar to the model-derived sea-ice data, we also evaluate the model's performance in depicting ocean tempera-

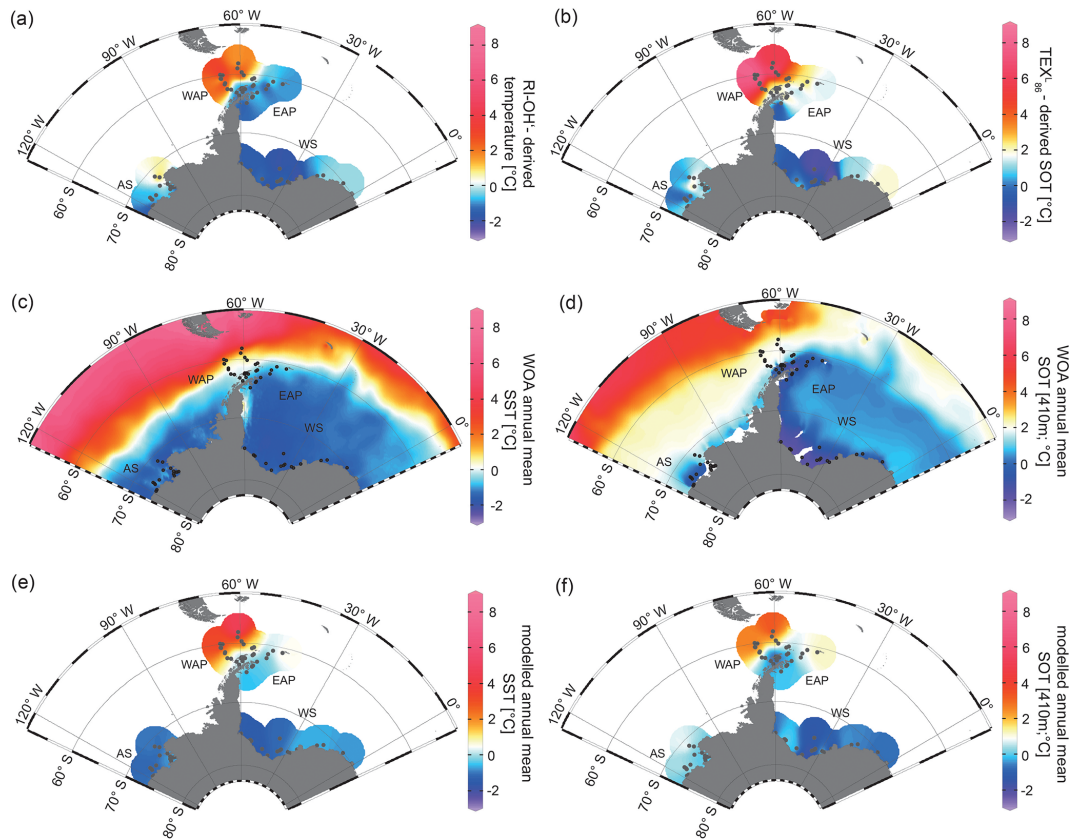


Figure 6. Annual mean temperature distributions with (a) RI-OH'-derived temperature, (b) TEX_{86}^L -derived SOT, (c) WOA13 SST (Locarnini et al., 2013), (d) WOA13 SOT (410 m; Locarnini et al., 2013), (e) modelled SST and (f) modelled SOT (410 m) in degrees Celsius. The following abbreviations are used in the figure: AS – Amundsen Sea, WAP – West Antarctic Peninsula, EAP – East Antarctic Peninsula and WS – Weddell Sea. Maps were generated using the Ocean Data View Software (Schlitzer, 2017).

tures (Fig. 6e, f). Modelled annual mean SSTs and SOTs are highest (with up to 5 and 3 °C respectively) in the permanently ice-free Drake Passage, which is influenced by the relatively warm ACC. Lower SSTs are predicted for the Antarctic Peninsula continental slope and Bransfield Strait (~ 0.5 to 1 °C), coinciding with the increase in the duration of seasonal sea-ice cover in that area. At the EAP/northwestern Weddell Sea, modelled SSTs as well as SOTs increase from southwest to northeast towards Powell Basin. In the Amundsen and Weddell seas, annual mean SSTs are negative, with temperatures ranging from -1 to -0.5 °C, whereas SOTs are positive in the Amundsen Sea and negative in the Weddell Sea. Overall, we note that modelled SOTs reflect instrumental SOTs reasonably well ($R^2 = 0.76$; Fig. 7d). Interestingly, while RI-OH'-derived SOTs relate better to instrumental SOTs (than TEX_{86}^L -based SOTs), a better correlation between TEX_{86}^L -derived SOTs and modelled SOTs ($R^2 = 0.64$; Fig. 7e) and a weaker correlation with RI-OH'-derived temperatures ($R^2 = 0.55$; Fig. 7f) is found.

5 Caveats and recommendations for future research

Marine core-top studies evaluating the applicability and reliability of climate proxies are often affected by limitations and uncertainties regarding the age control of the investigated seafloor surface sediments as well as the production, preservation and degradation of target compounds. In the following, we briefly address some of these factors and provide recommendations for future investigations.

5.1 Age control

Information on the actual age of the surface sediment samples is a major requirement determining their suitability to reflect modern sea surface conditions. When comparing sea-ice conditions or ocean temperatures estimated from biomarker data obtained from 0.5–1 cm thick surface sediment samples (easily spanning decades to millennia, depending on sedimentation rates) with satellite-derived sea-ice data or instrumental records (covering only the past ~ 40 and 65 years respectively), the different time periods reflected in the data sets need to be considered when interpreting the results.

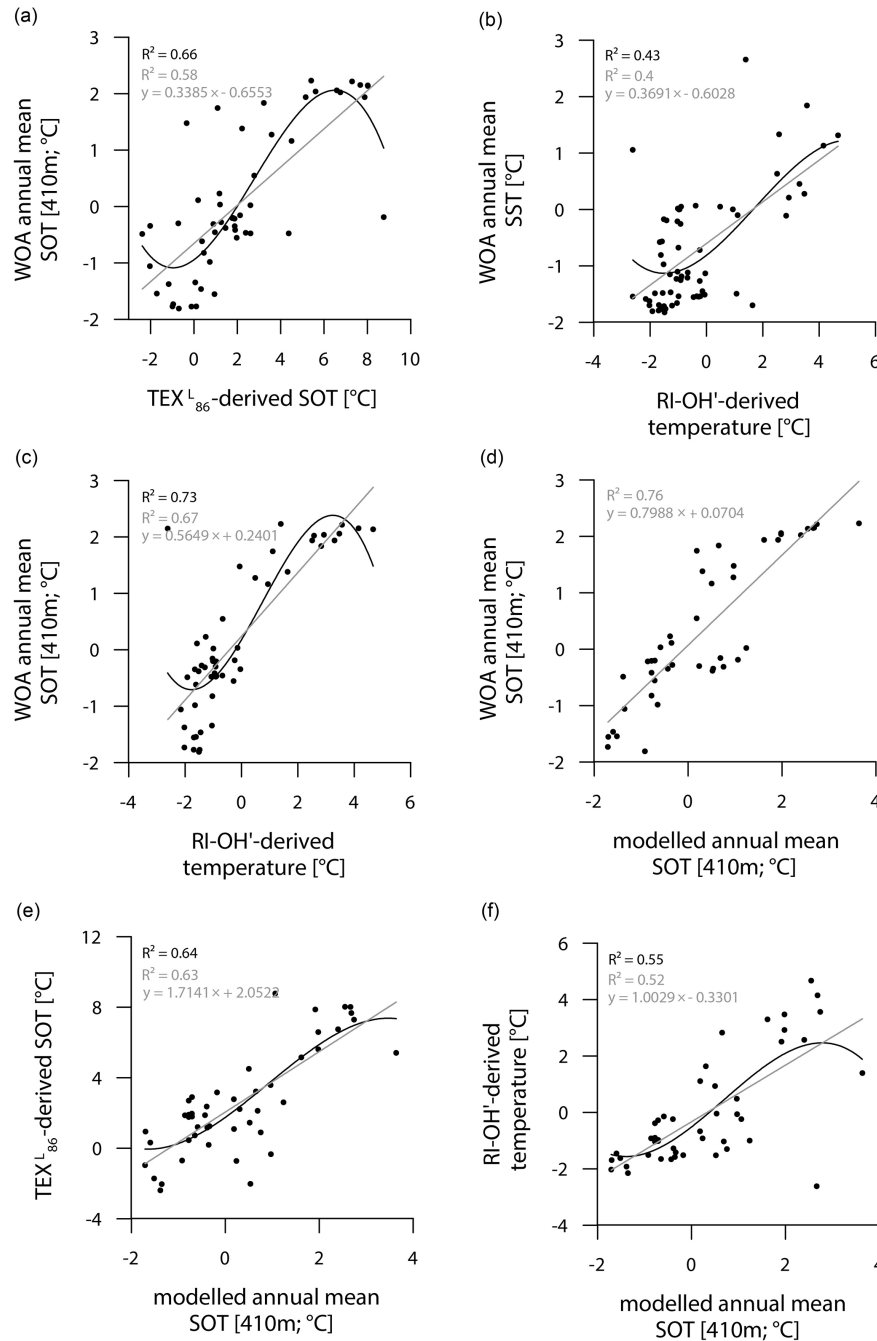


Figure 7. Correlations of (a) WOA annual mean SOT (410 m) vs. TEX_{86}^L -derived SOT, (b) WOA annual mean SST vs. RI-OH'-derived temperature, (c) WOA annual mean SOT (410 m) vs. RI-OH'-derived temperature, (d) WOA annual mean SOT (410 m) vs. modelled annual mean SOT (410 m), (e) TEX_{86}^L -derived SOT vs. modelled annual mean SOT (410 m) and (f) RI-OH'-derived temperature vs. modelled annual mean SOT (410 m) in degrees Celsius. Coefficients of determination (R^2) are given for the respective regression lines.

To address the issue of lacking age constraints for most of the surface sediments investigated here, we also performed palaeoclimate simulations providing sea-ice concentration data for three time slices (2 ka, 4 ka and 6 ka BP; see Fig. S5) to evaluate if the surface sediments may have recorded significantly older environmental conditions. Correlations of

PIPSO₂₅ values with these (palaeo-) sea-ice concentrations are notably weaker (Fig. S5) than the correlations with recent (1951–2014 CE) SIC model output, which points to a young to modern age of the majority of the studied sediments. This is further supported by AMS ¹⁴C dating of calcareous microfossils and ²¹⁰Pb dating of seafloor surface sediments from

the Amundsen Sea shelf documenting recent ages for most sites (Hillenbrand et al., 2010, 2013, 2017; Smith et al., 2011, 2014, 2017; Witus et al., 2014) as well as modern ^{210}Pb dates obtained for three multicores collected in Bransfield Strait (PS97/56, PS97/68 and PS97/72; Vorrath et al., 2020). AMS ^{14}C dates obtained for nearby seafloor surface sediments in the vicinity of the South Shetland Islands and the Antarctic Sound revealed ages of 100 and 142 years BP respectively (Vorrath et al., 2019). As both uncorrected ages lie within the range of the modern marine reservoir effect (e.g. Gordon and Harkness, 1992), we still consider these two dates as recent. However, in an area that has been significantly affected by rapid climate warming over the past decades and a regionally variable sea-ice coverage, the age uncertainties for at least ^{14}C -dated samples may easily lead to an over- or underestimation of biomarker-based sea-ice cover and ocean temperatures respectively, which needs to be taken into account for comparisons with instrumental data. The utilization of (palaeo-) model data may alleviate the lack of age control for each seafloor sediment sample to some extent. Nevertheless, we recommend that for a robust calibration of, for example, PIPSO₂₅ values against satellite-derived sea-ice concentrations, only surface sediment samples with a modern age confirmed by ^{210}Pb dating are incorporated.

5.2 Production and preservation of biomarkers

Biomarkers have the potential to reveal the former occurrence of their producers, which requires knowledge of the source organisms. While there is a general consensus on Thaumarchaeota being the major source of iso-GDGTs (Fietz et al., 2020, and references therein) and diatoms synthesizing HBIs (Volkman, 2006), the main source of brassicasterol, which is not only found in diatoms but also in dinoflagellates and haptophytes (Volkman, 2006), remains unclear. Accordingly, the use of brassicasterol to determine the PIPSO₂₅ index may introduce uncertainties regarding the environmental information recorded by this phytoplankton biomarker. A further aspect concerns the different chemical structures of HBIs and sterols, which raises the risk of a selective degradation (see Belt, 2018, Rontani et al., 2018, and Rontani et al., 2019, for detailed discussion) with potentially considerable effects on the PIPSO₂₅ index. Regarding the different areas investigated in our study, spatially different microbial communities and varying depositional regimes, such as sedimentation rate, redox conditions and water depth, may also lead to different degradation patterns. This means that variations in the biomarker concentrations between different areas may not strictly reflect changes in the production of these compounds (driven by sea surface conditions) but may also relate to different degradation states. In particular, lower sedimentation rates and, thus, extended oxygen exposure times promote chemical alteration and degradation processes (Hedges et al., 1999; Schouten et al., 2013). However, it has been previously reported that the formation of mineral

aggregates and fecal pellets often accelerates the transport of organic matter from the sea surface through the water column to the seafloor during the melting season, leading to a more rapid burial and, hence, better preservation of the organic compounds (Bauerfeind et al., 2005; Etourneau et al., 2019; Müller et al., 2011).

Another rather technical drawback concerning the use of the PIPSO₂₅ index occurs when the concentrations of the sea-ice proxy IPSO₂₅ and the phytoplankton marker are similarly low (due to unfavourable conditions for both ice algae and phytoplankton) or similarly high (due to a significant seasonal shift in sea-ice cover and/or stable ice edge conditions). This may lead to similar PIPSO₂₅ values, although the sea-ice conditions are fundamentally different from each other. This scenario is evident for five sampling sites in the Weddell Sea (PS111/13-2, /15-1, /16-3, /29-3 and /40-2; Fig. 3b, c), where IPSO₂₅ and the HBI Z-triene concentrations are close to the detection limit and P_ZIPSO₂₅ values are very low, suggesting a reduced sea-ice cover. Satellite and model data, however, show that these sample locations are influenced by heavy, nearly year-round sea-ice cover. We conclude that biomarker concentrations of both biomarkers at or close to the detection limit need to be treated with caution. Here, we assigned a maximum P_ZIPSO₂₅ value of 1 to those samples, and we note that such a practice always needs to be clarified when applying the PIPSO₂₅ approach. Nonetheless, the coupling of IPSO₂₅ with a phytoplankton marker provides more reliable sea-ice reconstructions. Regarding all these ambiguities, we recommend not only calculating the PIPSO₂₅ index but also to carefully considering individual biomarker concentrations and, if possible, to utilizing other sea-ice proxies, such as data from well-preserved diatom assemblages (Lamping et al., 2020; Vorrath et al., 2019, 2020). While the PIPSO₂₅ index is not yet a fully quantitative proxy for (palaeo-) sea-ice concentrations, several calibration iterations have been applied to the GDGT palaeothermometers (Fietz et al., 2020). As noted above, the observation of distinctly warm-biased TEX₈₆^L-derived SOTs calls for further efforts such as regional calibration studies and/or investigations of archaean adaptation strategies at different water depths and under different nutrient and temperature conditions.

5.3 The role of platelet ice for the production of IPSO₂₅

The sympagic, tube-dwelling, diatom *B. adeliensis* is a common constituent of Antarctic sea ice and preferably flourishes in the relatively open channels of sub-ice platelet layers in near-shore locations covered by fast ice (Medlin, 1990; Riaux-Gobin and Poulin, 2004). Based on investigations of sea-ice samples from the Southern Ocean, Belt et al. (2016) detected this diatom species to be a source of IPSO₂₅, which, according to its habitat, led to the assumption of the sea-ice proxy being a potential indicator for the presence of platelet ice. As stated above, *B. adeliensis* is not confined to platelet

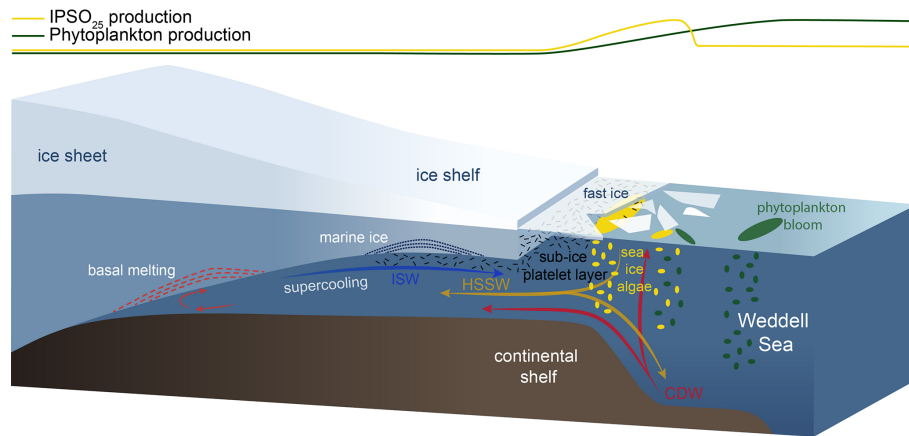


Figure 8. Schematic illustration of the formation of platelet ice and the main production areas of sea-ice algae producing IPSO₂₅ (yellow ellipses) and phytoplankton (green ellipses), also displayed by yellow and green curves at the top of the figure. The following abbreviations are used in the figure: CDW – Circumpolar Deep Water, HSSW – High Saline Shelf Water and ISW – Ice Shelf Water. Illustration modified from Scambos et al. (2017).

ice and is also observed in basal sea ice and described as well adapted to changes in the texture of sea ice during ice melt (Riaux-Gobin et al., 2013). Platelet ice formation, however, plays an important role in sea-ice generation along some coastal regions of Antarctica (Hoppmann et al., 2015, 2020; Lange et al., 1989; Langhorne et al., 2015). In these regions, CDW and High Saline Shelf Water (HSSW) flow into sub-ice-shelf cavities of ice shelves and cause basal melting and the discharge of cold and less saline water (Fig. 8; Hoppmann et al., 2020; Scambos et al., 2017). The surrounding water is cooled and freshened and is then transported towards the surface. Under the large Filchner–Ronne and Ross ice shelves, the pressure relief can cause this water, called Ice Shelf Water (ISW), to be supercooled (Foldvik and Kvinge, 1974). The temperature of the supercooled ISW is typically below the in situ freezing point, which eventually causes the formation of ice platelets that accumulate under landfast ice attached to adjacent ice shelves (Fig. 8; Holland et al., 2007; Hoppmann et al., 2015, 2020).

In an attempt to elucidate the relationship between IPSO₂₅ and platelet ice, we investigated our data with respect to the locations of observed platelet ice formation. While the maximum IPSO₂₅ concentrations in front of the Filchner Ice Shelf could be directly related to the above-mentioned platelet ice formation in this area, the elevated IPSO₂₅ concentrations north of the Larsen C Ice Shelf at the EAP could be linked to several processes. According to Langhorne et al. (2015), sea-ice cores retrieved from that area did not incorporate platelet ice. Hence, the high IPSO₂₅ concentrations could be explained by either input from drift ice transported with the Weddell Gyre or by basal freeze-on. However, we note that our samples may reflect much longer time periods than the sea-ice samples investigated by Langhorne et al. (2015), and the lack of platelet ice in their investigated sea-ice cores does

not rule out the former presence of platelet ice, which may be captured in our investigated sediment samples.

There are several previous studies on IPSO₂₅ that reported a close connection of the proxy with proximal, coastal locations and polynyas in the seasonal ice zone (i.e. Collins et al., 2013; Smik et al., 2016). They do not, however, discuss the relation to adjacent ice shelves as possible “platelet ice factories”. We note that the core locations investigated by Smik et al. (2016) are in the vicinity of the Moscow University Ice Shelf, where Langhorne et al. (2015) did not observe platelet ice within sea-ice cores. Hoppmann et al. (2020), however, report a sea-ice core from that area, which incorporates platelet ice. The different observations by Langhorne et al. (2015) and Hoppmann et al. (2020) highlight the temporal variability in the occurrence of platelet ice in the cold-water regime around the East Antarctic margin.

For the observed IPSO₂₅ minimum in the Amundsen Sea (AS, Fig. 3b), which we tentatively relate to the extended and thick sea-ice coverage, the absence of platelet ice there is an alternative explanation. The Amundsen/Bellinghousen seas and WAP shelves are classified as “warm shelves” (Thompson et al., 2018), where the upwelling of warm CDW (Schmidtko et al., 2014) hinders the formation of ISW, which makes the presence of platelet ice under recent conditions highly unlikely (Hoppmann et al., 2020). This is also supported by Langhorne et al. (2015), who stated that platelet ice formation is not observed in areas where basal ice-shelf melting is considerable, such as on the West Antarctic continental shelf in the eastern Pacific sector of the Southern Ocean (Thompson et al., 2018). Accordingly, if the formation and accumulation of platelet ice – up to a certain degree – indicates sub-ice-shelf melting on “cold shelves” (Hoppmann et al., 2015; Thompson et al., 2018), high IPSO₂₅ concentrations found in marine sediments may serve as an indicator of past ISW formation and associated ice-shelf dynamics.

This is, however, probably only true up to a certain threshold, where platelet ice formation decreases or is hampered due to warm oceanic conditions causing overly intense sub-ice-shelf melting (Langhorne et al., 2015).

When using IPSO₂₅ as a sea-ice proxy in Antarctica, it is important to consider regional platelet ice formation processes too, as these may affect the IPSO₂₅ budget. Determining thresholds associated with platelet ice formation is challenging. Therefore, further investigations, such as in situ measurements of IPSO₂₅ concentrations in platelet ice or culture experiments in laboratories, are needed to better understand the connection between IPSO₂₅ and platelet ice formation (and basal ice-shelf melting).

6 Conclusions

Biomarker analyses focusing on IPSO₂₅, HBI-trienes, phytosterols and GDGTs in surface sediment samples from the Antarctic continental margin were investigated to depict recent sea-ice conditions and ocean temperatures in this climate-sensitive region. Proxy-based reconstructions of these key variables were compared to (1) satellite sea-ice data, (2) instrumental ocean temperature data, and (3) modelled sea-ice patterns and ocean temperatures. The semi-quantitative sea-ice index PIPSO₂₅, combining the sea-ice proxy IPSO₂₅ with an open-water phytoplankton marker, yielded reasonably good correlations with satellite observations and numerical model results, whereas correlations with the sea-ice proxy IPSO₂₅ alone are rather low. Minimum concentrations of both biomarkers, used for the PIPSO₂₅ calculations, may lead to ambiguous interpretations and significant underestimations of sea-ice conditions. Therefore, different sea-ice measures should be considered when interpreting biomarker data.

Ocean temperature reconstructions based on the TEX₈₆^L and RI-OH' palaeothermometers show similar patterns, but different absolute temperatures. While TEX₈₆^L-derived temperatures are significantly biased towards warm temperatures in Drake Passage, the RI-OH'-derived temperature range seems more realistic when compared to temperature data based on the WOA13 and modelled annual mean SOTs.

Further investigations of HBI- as well as GDGT-synthesis, transport, deposition and preservation within the sediments would help to guide the proxies' application. Further work on the taxonomy of the IPSO₂₅ producers, the composition of their habitat (basal sea ice, platelet ice, brine channels) and their connection to platelet ice formation via in situ or laboratory measurements are required to better constrain the IPSO₂₅ potential as a robust sea-ice biomarker. The presumed relationship between IPSO₂₅ and platelet ice formation in connection to sub-ice-shelf melting is supported by our data, showing high IPSO₂₅ concentrations in areas with known platelet ice formation and low IPSO₂₅ concentrations in areas without observed platelet ice formation. Accord-

ingly, oceanic conditions and the intensity of sub-ice-shelf melting need to be considered when using IPSO₂₅ (1) as an indirect indicator for sub-ice-shelf melting processes and associated ice-shelf dynamics and (2) for the application of the PIPSO₂₅ index to estimate sea-ice coverage.

Data availability. Data sets related to this article can be found online on the PANGAEA Data Publisher for Earth & Environmental Science. (<https://doi.org/10.1594/PANGAEA.932265>; Lamping et al., 2021).

Supplement. The supplement related to this article is available online at: <https://doi.org/10.5194/cp-17-2305-2021-supplement>.

Author contributions. NL and JM designed the concept of the study. NL carried out biomarker experiments. XS and GL developed the model code, and XS performed the simulations. CH provided the satellite data. MEV provided hitherto unpublished glycerol dialkyl glycerol tetraether data for PS97 samples. GM and JH carried out the glycerol dialkyl glycerol tetraether analyses. CDH collected surface sediment samples and advised on their ages. NL prepared the paper and visualizations with contributions from all co-authors.

Competing interests. The authors declare that they have no conflict of interest.

Disclaimer. Publisher's note: Copernicus Publications remains neutral with regard to jurisdictional claims in published maps and institutional affiliations.

Special issue statement. This article is part of the special issue "Reconstructing Southern Ocean sea-ice dynamics on glacial-to-historical timescales". It is not associated with a conference.

Acknowledgements. Denise Diekstatt, Mandy Kuck and Jonas Haase are kindly acknowledged for laboratory support. We thank the captains, crews and science parties of RV *Polarstern* cruises PS69, PS97, PS104, PS111 and PS118. Specifically, Frank Niessen, Sabine Hanisch and Michael Schreck are thanked for their support during PS118. Simon Belt is acknowledged for providing the 7-HND internal standard for HBI quantification. AWI, MARUM – University of Bremen, the British Antarctic Survey and NERC UK-IODP are acknowledged for funding expedition PS104. Nele Lamping, Maria-Elena Vorrath and Juliane Müller were funded through the Helmholtz-Gemeinschaft. The two anonymous reviewers are thanked for their constructive and helpful comments, which led to a significant improvement in this paper.

Financial support. This research has been supported by the Helmholtz-Gemeinschaft (grant no. VH-NG-1101).

The article processing charges for this open-access publication were covered by the Alfred Wegener Institute, Helmholtz Centre for Polar and Marine Research (AWI).

Review statement. This paper was edited by Xavier Crosta and reviewed by two anonymous referees.

References

- Abernathy, R. P., Cerovecki, I., Holland, P. R., Newsom, E., Mazloff, M., and Talley, L. D.: Water-mass transformation by sea ice in the upper branch of the Southern Ocean overturning, *Nat. Geosci.*, 9, 596–601, 2016.
- Allen, C. S., Pike, J., and Pudsey, C. J.: Last glacial-interglacial sea-ice cover in the SW Atlantic and its potential role in global deglaciation, *Quaternary Sci. Rev.*, 30, 2446–2458, 2011.
- Alonso-Sáez, L., Andersson, A., Heinrich, F., and Bertilsson, S.: High archaeal diversity in Antarctic circumpolar deep waters, *Env. Microbiol. Rep.*, 3, 689–697, 2011.
- Anderson, P. S.: Evidence for an Antarctic winter coastal polynya, *Antarct. Sci.*, 5, 221–226, 1993.
- Armand, L. K. and Leventer, A.: Palaeo sea ice distribution-reconstruction and palaeoclimatic significance, in: *Sea ice – an introduction to its physics, biology, chemistry, and geology*, edited by: Thomas, D. N. and Dieckmann, G. S., Wiley-Blackwell, Hoboken, New Jersey, ch. 11, 333–372, 2003.
- Arndt, J. E., Schenke, H. W., Jakobsson, M., Nitsche, F. O., Buys, G., Goleby, B., Rebesco, M., Bohoyo, F., Hong, J., Black, J., Greku, R., Udintsev, G., Barrios, F., Reynoso-Peralta, W., Taisei, M., and Wigley, R.: The International Bathymetric Chart of the Southern Ocean (IBCSO) Version 1.0 – A new bathymetric compilation covering circum-Antarctic waters, *Geophys. Res. Lett.*, 40, 3111–3117, 2013.
- Arrigo, K. R.: Sea ice as a habitat for primary producers, *Sea ice*, 276, 352–369, 2017.
- Arrigo, K. R., Worthen, D. L., Lizotte, M. P., Dixon, P., and Dieckmann, G.: Primary production in Antarctic sea ice, *Science*, 276, 394–397, 1997.
- Barbara, L., Crosta, X., Schmidt, S., and Massé, G.: Diatoms and biomarkers evidence for major changes in sea ice conditions prior the instrumental period in Antarctic Peninsula, *Quaternary Sci. Rev.*, 79, 99–110, 2013.
- Bauerfeind, E., Leipe, T., and Ramseier, R. O.: Sedimentation at the permanently ice-covered Greenland continental shelf (74°57.7' N/12°58.7' W): significance of biogenic and lithogenic particles in particulate matter flux, *J. Marine Syst.*, 56, 151–166, 2005.
- Belt, S. T.: Source-specific biomarkers as proxies for Arctic and Antarctic sea ice, *Org. Geochem.*, 125, 277–298, 2018.
- Belt, S. T. and Müller, J.: The Arctic sea ice biomarker IP₂₅: a review of current understanding, recommendations for future research and applications in palaeo sea ice reconstructions, *Quaternary Sci. Rev.*, 79, 9–25, 2013.
- Belt, S. T., Allard, W. G., Massé, G., Robert, J.-M., and Rowland, S. J.: Highly branched isoprenoids (HBIs): identification of the most common and abundant sedimentary isomers, *Geochim. Cosmochim. Ac.*, 64, 3839–3851, 2000.
- Belt, S. T., Brown, T. A., Ampel, L., Cabedo-Sanz, P., Fahl, K., Kocis, J. J., Massé, G., Navarro-Rodriguez, A., Ruan, J., and Xu, Y.: An inter-laboratory investigation of the Arctic sea ice biomarker proxy IP₂₅ in marine sediments: key outcomes and recommendations, *Clim. Past*, 10, 155–166, <https://doi.org/10.5194/cp-10-155-2014>, 2014.
- Belt, S. T., Cabedo-Sanz, P., Smik, L., Navarro-Rodriguez, A., Berben, S. M. P., Knies, J., and Husum, K.: Identification of paleo Arctic winter sea ice limits and the marginal ice zone: Optimised biomarker-based reconstructions of late Quaternary Arctic sea ice, *Earth. Planet. Sc. Lett.*, 431, 127–139, 2015.
- Belt, S. T., Smik, L., Brown, T. A., Kim, J. H., Rowland, S. J., Allen, C. S., Gal, J. K., Shin, K. H., Lee, J. I., and Taylor, K. W. R.: Source identification and distribution reveals the potential of the geochemical Antarctic sea ice proxy IPSO₂₅, *Nat. Commun.*, 7, 12655, <https://doi.org/10.1038/ncomms12655>, 2016.
- Belt, S. T., Brown, T. A., Smik, L., Tatarek, A., Wiktor, J., Stowasser, G., Assmy, P., Allen, C. S., and Husum, K.: Identification of C₂₅ highly branched isoprenoid (HBI) alkenes in diatoms of the genus *Rhizosolenia* in polar and sub-polar marine phytoplankton, *Org. Geochem.*, 110, 65–72, 2017.
- Berger, A.: Long-term variations of daily insolation and Quaternary climatic changes, *J. Atmos. Sci.*, 35, 2362–2367, 1978.
- Blain, S., Quéguiner, B., Armand, L., Belviso, S., Bombled, B., Bopp, L., Bowie, A., Brunet, C., Brussaard, C., Carlotti, F., Christaki, U., Corbière, A., Durand, I., Ebersbach, F., Fuda, J.-L., Garcia, N., Gerringa, L., Griffiths, B., Guigue, C., Guillermin, C., Jacquet, S., Jeandel, C., Laan, P., Lefèvre, D., Lo Monaco, C., Malits, A., Mosseri, J., Obernosterer, I., Park, Y.-H., Picheral, M., Pondaven, P., Remenyi, T., Sandroni, V., Sarthou, G., Savoye, N., Scouarnec, L., Souhaut, M., Thuiller, D., Timmermans, K., Trull, T., Uitz, J., van Beek, P., Veldhuis, M., Vincent, D., Viollier, E., Vong, L., and Wagener, T.: Effect of natural iron fertilization on carbon sequestration in the Southern Ocean, *Nature*, 446, 1070–1074, 2007.
- Boon, J. J., Rijpstra, W. I. C., de Lange, F., De Leeuw, J., Yoshioka, M., and Shimizu, Y.: Black Sea sterol—a molecular fossil for dinoflagellate blooms, *Nature*, 277, 125–127, 1979.
- Cárdenas, P., Lange, C. B., Vernet, M., Esper, O., Srain, B., Vorrath, M.-E., Ehrhardt, S., Müller, J., Kuhn, G., and Arz, H. W.: Biogeochemical proxies and diatoms in surface sediments across the Drake Passage reflect oceanic domains and frontal systems in the region, *Prog. Oceanogr.*, 174, 72–88, 2019.
- Cavaliere, D., Parkinson, C., Gloersen, P., and Zwally, H.: Sea ice concentrations from Nimbus-7 SMMR and DMSP SSM/I passive microwave data, National Snow and Ice Data Center, Boulder, Colorado, USA, <https://doi.org/10.1029/1999JC900081>, 1996.
- Collares, L. L., Mata, M. M., Kerr, R., Arigony-Neto, J., and Barbat, M. M.: Iceberg drift and ocean circulation in the northwestern Weddell Sea, Antarctica, *Deep-Sea Res. Pt. II*, 149, 10–24, 2018.
- Colleoni, F., De Santis, L., Siddoway, C. S., Bergamasco, A., Golledge, N. R., Lohmann, G., Passchier, S., and Siegert, M. J.: Spatio-temporal variability of processes across

- Antarctic ice-bed–ocean interfaces, *Nat. Commun.*, 9, 2289, <https://doi.org/10.1038/s41467-018-04583-0>, 2018.
- Collins, L. G., Allen, C. S., Pike, J., Hodgson, D. A., Weckström, K., and Massé, G.: Evaluating highly branched isoprenoid (HBI) biomarkers as a novel Antarctic sea-ice proxy in deep ocean glacial age sediments, *Quaternary Sci. Rev.*, 79, 87–98, 2013.
- Comiso, J. C., Gersten, R. A., Stock, L. V., Turner, J., Perez, G. J., and Cho, K.: Positive Trend in the Antarctic Sea Ice Cover and Associated Changes in Surface Temperature, *J. Climate.*, 30, 2251–2267, 2017.
- Cook, A. J., Holland, P., Meredith, M., Murray, T., Luckman, A., and Vaughan, D. G.: Ocean forcing of glacier retreat in the WAP, *Science*, 353, 283–286, 2016.
- Crosta, X., Pichon, J. J., and Burckle, L.: Application of modern analog technique to marine Antarctic diatoms: Reconstruction of maximum sea-ice extent at the Last Glacial Maximum, *Paleoceanography and Paleoclimatology*, 13, 284–297, 1998.
- Crosta, X., Etourneau, J., Orme, L. C., Dalaiden, Q., Campagne, P., Swingedouw, D., Goosse, H., Massé, G., Miettinen, A., McKay, R. M., Dunbar, R. B., Escutia, C., and Ikehara, M.: Multi-decadal trends in Antarctic sea-ice extent driven by ENSO–SAM over the last 2000 years, *Nat. Geosci.*, 14, 156–160, 2021.
- Danilov, S., Sidorenko, D., Wang, Q., and Jung, T.: The Finite-volume Sea ice–Ocean Model (FESOM2), *Geosci. Model Dev.*, 10, 765–789, <https://doi.org/10.5194/gmd-10-765-2017>, 2017.
- De Jong, J., Schoemann, V., Lannuzel, D., Croot, P., de Baar, H., and Tison, J. L.: Natural iron fertilization of the Atlantic sector of the Southern Ocean by continental shelf sources of the Antarctic Peninsula, *J. Geophys. Res.-Biogeo.*, 117, G01029, <https://doi.org/10.1029/2011JG001679>, 2012.
- Denis, D., Crosta, X., Barbara, L., Massé, G., Renssen, H., Ther, O., and Giraudeau, J.: Sea ice and wind variability during the Holocene in East Antarctica: insight on middle–high latitude coupling, *Quaternary Sci. Rev.*, 29, 3709–3719, 2010.
- Dorschel, B.: The Expedition PS118 of the Research Vessel *POLARSTERN* to the Weddell Sea in 2019, *Berichte zur Polar- und Meeresforschung, Reports on Polar and Marine Research, Alfred-Wegener-Institut für Polar- und Meeresforschung, Bremerhaven, Germany*, 735, 149 pp., 2019.
- Doty, M. S. and Oguri, M.: The island mass effect, *ICES J. Mar. Sci.*, 22, 33–37, 1956.
- Eayrs, C., Li, X., Raphael, M. N., and Holland, D. M.: Rapid decline in Antarctic sea ice in recent years hints at future change, *Nat. Geosci.*, 14, 460–464, 2021.
- Esper, O. and Gersonde, R.: New tools for the reconstruction of Pleistocene Antarctic sea ice, *Palaeogeogr. Palaeocl.*, 399, 260–283, 2014.
- Etourneau, J., Collins, L. G., Willmott, V., Kim, J.-H., Barbara, L., Leventer, A., Schouten, S., Sinninghe Damsté, J. S., Bianchini, A., Klein, V., Crosta, X., and Massé, G.: Holocene climate variations in the western Antarctic Peninsula: evidence for sea ice extent predominantly controlled by changes in insolation and ENSO variability, *Clim. Past*, 9, 1431–1446, <https://doi.org/10.5194/cp-9-1431-2013>, 2013.
- Etourneau, J., Sgubin, G., Crosta, X., Swingedouw, D., Willmott, V., Barbara, L., Houssais, M.-N., Schouten, S., Damsté, J. S. S., and Goosse, H.: Ocean temperature impact on ice shelf extent in the eastern Antarctic Peninsula, *Nat. Commun.*, 10, 1–8, 2019.
- Fahl, K. and Stein, R.: Modern seasonal variability and deglacial/Holocene change of central Arctic Ocean sea-ice cover: new insights from biomarker proxy records, *Earth. Planet. Sc. Lett.*, 351, 123–133, 2012.
- Fetterer, F., Knowles, K., Meier, W., Savoie, M., and Windnagel, A. K.: Updated Daily, Sea Ice Index, Version 2. [Median Sea Ice Extent 1981–2010], NSIDC: National Snow and Ice Data Center [data set], Boulder, Colorado USA, <https://doi.org/10.7265/N5736NV7> (last access: 24 July 2017), 2016.
- Fietz, S., Hugué, C., Rueda, G., Hambach, B., and Rosell-Melé, A.: Hydroxylated isoprenoidal GDGTs in the Nordic Seas, *Mar. Chem.*, 152, 1–10, 2013.
- Fietz, S., Ho, S., and Hugué, C.: Archaeal Membrane Lipid-Based Paleothermometry for Applications in Polar Oceans, *Oceanography*, 33, 104–114, 2020.
- Foldvik, A. and Kvinge, T.: Conditional instability of sea water at the freezing point, *Deep.-Sea Res.*, 21, 169–174, 1974.
- Fretwell, P., Pritchard, H. D., Vaughan, D. G., Bamber, J. L., Barand, N. E., Bell, R., Bianchi, C., Bingham, R. G., Blankenship, D. D., Casassa, G., Catania, G., Callens, D., Conway, H., Cook, A. J., Corr, H. F. J., Damaske, D., Damm, V., Ferraccioli, F., Forsberg, R., Fujita, S., Gim, Y., Gogineni, P., Griggs, J. A., Hindmarsh, R. C. A., Holmlund, P., Holt, J. W., Jacobel, R. W., Jenkins, A., Jokat, W., Jordan, T., King, E. C., Kohler, J., Krabill, W., Riger-Kusk, M., Langley, K. A., Leitchenkov, G., Leuschen, C., Luyendyk, B. P., Matsuoka, K., Mouginot, J., Nitsche, F. O., Nogi, Y., Nost, O. A., Popov, S. V., Rignot, E., Rippon, D. M., Rivera, A., Roberts, J., Ross, N., Siegert, M. J., Smith, A. M., Steinhage, D., Studinger, M., Sun, B., Tinto, B. K., Welch, B. C., Wilson, D., Young, D. A., Xiangbin, C., and Zirizzotti, A.: Bedmap2: improved ice bed, surface and thickness datasets for Antarctica, *The Cryosphere*, 7, 375–393, <https://doi.org/10.5194/tc-7-375-2013>, 2013.
- Gersonde, R. and Zielinski, U.: The reconstruction of late Quaternary Antarctic sea-ice distribution—the use of diatoms as a proxy for sea-ice, *Palaeogeogr. Palaeocl.*, 162, 263–286, 2000.
- Gohl, K.: The expedition ANTARKTIS-XXIII/4 of the research vessel *Polarstern* in 2006, *Berichte zur Polar- und Meeresforschung (Reports on Polar and Marine Research), Alfred-Wegener-Institut für Polar- und Meeresforschung, Bremerhaven, Germany*, 557, 166 pp., 2007.
- Gohl, K.: The Expedition PS104 of the Research Vessel *POLARSTERN* to the Amundsen Sea in 2017, *Berichte zur Polar- und Meeresforschung (Reports on Polar and Marine Research), Alfred-Wegener-Institut für Polar- und Meeresforschung, Bremerhaven, Germany*, 712, 100 pp., 2017.
- Gordon, J. E. and Harkness, D. D.: Magnitude and geographic variation of the radiocarbon content in Antarctic marine life: implications for reservoir corrections in radiocarbon dating, *Quaternary Sci. Rev.*, 11, 697–708, 1992.
- Hancke, K., Lund-Hansen, L. C., Lamare, M. L., Højlund Pedersen, S., King, M. D., Andersen, P., and Sorrell, B. K.: Extreme low light requirement for algae growth underneath sea ice: A case study from Station Nord, NE Greenland, *J. Geophys. Res.-Oceans.*, 123, 985–1000, 2018.
- Harms, S., Fahrbach, E., and Strass, V. H.: Sea ice transports in the Weddell Sea, *J. Geophys. Res.-Oceans.*, 106, 9057–9073, 2001.

- Hedges, J. I., Hu, F. S., Devol, A. H., Hartnett, H. E., Tsamakis, E., and Keil, R. G.: Sedimentary organic matter preservation; a test for selective degradation under oxic conditions, *Am. J. Sci.*, 299, 529–555, 1999.
- Hellmer, H. H., Rhein, M., Heinemann, G., Abalichin, J., Abouchami, W., Baars, O., Cubasch, U., Dethloff, K., Ebner, L., Fahrbach, E., Frank, M., Gollan, G., Greatbatch, R. J., Grieger, J., Gryanik, V. M., Gryscha, M., Hauck, J., Hoppema, M., Huhn, O., Kanzow, T., Koch, B. P., König-Langlo, G., Langematz, U., Leckebusch, G. C., Lüpkes, C., Paul, S., Rinke, A., Rost, B., van der Loeff, M. R., Schröder, M., Seckmeyer, G., Stichel, T., Strass, V., Timmermann, R., Trimborn, S., Ulbrich, U., Venchiarutti, C., Wacker, U., Willmes, S., and Wolf-Gladrow, D.: Meteorology and oceanography of the Atlantic sector of the Southern Ocean – a review of German achievements from the last decade, *Ocean Dynam.*, 66, 1379–1413, 2016.
- Hillenbrand, C.-D., Smith, J. A., Kuhn, G., Esper, O., Gersonde, R., Larter, R. D., Maher, B., Moreton, S. G., Shimmield, T. M., and Korte, M.: Age assignment of a diatomaceous ooze deposited in the western Amundsen Sea Embayment after the Last Glacial Maximum, *J. Quaternary Sci.*, 25, 280–295, 2010.
- Hillenbrand, C.-D., Kuhn, G., Smith, J. A., Gohl, K., Graham, A. G. C., Larter, R. D., Klages, J. P., Downey, R., Moreton, S. G., Forwick, M., and Vaughan, D. G.: Grounding-line retreat of the West Antarctic Ice Sheet from inner Pine Island Bay, *Geology*, 41, 35–38, 2013.
- Hillenbrand, C.-D., Smith, J. A., Hodell, D. A., Greaves, M., Poole, C. R., Kender, S., Williams, M., Andersen, T. J., Jernas, P. E., Elderfield, H., Klages, J. P., Roberts, S. J., Gohl, K., Larter, R. D., and Kuhn, G.: West Antarctic Ice Sheet retreat driven by Holocene warm water intrusions, *Nature*, 547, 43–48, 2017.
- Hobbs, W. R., Massom, R., Stammerjohn, S., Reid, P., Williams, G., and Meier, W.: A review of recent changes in Southern Ocean sea ice, their drivers and forcings, *Global Planet. Change.*, 143, 228–250, 2016.
- Holland, P. R., Feltham, D. L., and Jenkins, A.: Ice shelf water plume flow beneath Filchner-Ronne Ice Shelf, Antarctica, *J. Geophys. Res.-Oceans.*, 112, C05044, <https://doi.org/10.1029/2006JC003915>, 2007.
- Hoppmann, M., Nicolaus, M., Paul, S., Hunkeler, P. A., Heinemann, G., Willmes, S., Timmermann, R., Boebel, O., Schmidt, T., and Kühnel, M.: Ice platelets below Weddell Sea landfast sea ice, *Ann. Glaciol.*, 56, 175–190, 2015.
- Hoppmann, M., Richter, M. E., Smith, I. J., Jendersie, S., Langhorne, P. J., Thomas, D. N., and Dieckmann, G. S.: Platelet ice, the Southern Ocean's hidden ice: a review, *Ann. Glaciol.*, 61, 1–28, 2020.
- Hopmans, E. C., Weijers, J. W., Schefuß, E., Herfort, L., Damsté, J. S. S., and Schouten, S.: A novel proxy for terrestrial organic matter in sediments based on branched and isoprenoid tetraether lipids, *Earth. Planet. Sc. Lett.*, 224, 107–116, 2004.
- Huguet, C., de Lange, G. J., Gustafsson, Ö., Middelburg, J. J., Damsté, J. S. S., and Schouten, S.: Selective preservation of soil organic matter in oxidized marine sediments (Madeira Abyssal Plain), *Geochim. Cosmochim. Ac.*, 72, 6061–6068, 2008.
- Huguet, C., Fietz, S., Rosell-Melé, A., Daura, X., and Costenaro, L.: Molecular dynamics simulation study of the effect of glycerol dialkyl glycerol tetraether hydroxylation on membrane thermostability, *BBA-Biomembranes*, 1859, 966–974, 2017.
- Iacono, M. J., Delamere, J. S., Mlawer, E. J., Shephard, M. W., Clough, S. A., and Collins, W. D.: Radiative forcing by long-lived greenhouse gases: Calculations with the AER radiative transfer models, *J. Geophys. Res.-Atmos.*, 113, D13103, <https://doi.org/10.1029/2008JD009944>, 2008.
- Jacobs, S. S., Jenkins, A., Giulivi, C. F., and Dutrieux, P.: Stronger ocean circulation and increased melting under Pine Island Glacier ice shelf, *Nat. Geosci.*, 4, 519–523, 2011.
- Jenkins, A. and Jacobs, S.: Circulation and melting beneath George VI ice shelf, Antarctica, *J. Geophys. Res.-Oceans.*, 113, C04013, <https://doi.org/10.1029/2007JC004449>, 2008.
- Jenkins, A., Shoosmith, D., Dutrieux, P., Jacobs, S., Kim, T. W., Lee, S. H., Ha, H. K., and Stammerjohn, S.: West Antarctic Ice Sheet retreat in the Amundsen Sea driven by decadal oceanic variability, *Nature Geoscience*, 11, 733–738, 2018.
- Johns, L., Wraige, E., Belt, S., Lewis, C., Massé, G., Robert, J.-M., and Rowland, S.: Identification of a C₂₅ highly branched isoprenoid (HBI) diene in Antarctic sediments, Antarctic sea-ice diatoms and cultured diatoms, *Org. Geochem.*, 30, 1471–1475, 1999.
- Kalanetra, K. M., Bano, N., and Hollibaugh, J. T.: Ammonia-oxidizing Archaea in the Arctic Ocean and Antarctic coastal waters, *Environ. Microbiol.*, 11, 2434–2445, 2009.
- Khazendar, A., Rignot, E., Schroeder, D. M., Seroussi, H., Schodlok, M. P., Scheuchl, B., Mouginot, J., Sutterley, T. C., and Velicogna, I.: Rapid submarine ice melting in the grounding zones of ice shelves in West Antarctica, *Nat. Commun.*, 7, 1–8, 2016.
- Kim, J.-H., Van der Meer, J., Schouten, S., Helmke, P., Willmott, V., Sangiorgi, F., Koç, N., Hopmans, E. C., and Damsté, J. S. S.: New indices and calibrations derived from the distribution of crenarchaeal isoprenoid tetraether lipids: Implications for past sea surface temperature reconstructions, *Geochim. Cosmochim. Ac.*, 74, 4639–4654, 2010.
- Kim, J.-H., Crosta, X., Willmott, V., Renssen, H., Bonnin, J., Helmke, P., Schouten, S., and Damsté, J. S. S.: Holocene subsurface temperature variability in the eastern Antarctic continental margin, *Geophys. Res. Lett.*, 39, L06705, <https://doi.org/10.1029/2012GL051157>, 2012.
- Klinck, J. M., Hofmann, E. E., Beardsley, R. C., Salihoglu, B., and Howard, S.: Water-mass properties and circulation on the WAP Continental Shelf in Austral Fall and Winter 2001, *Deep-Sea Res. Pt. II.*, 51, 1925–1946, 2004.
- Köhler, P., Nehrbass-Ahles, C., Schmitt, J., Stocker, T. F., and Fischer, H.: A 156 kyr smoothed history of the atmospheric greenhouse gases CO₂, CH₄, and N₂O and their radiative forcing, *Earth Syst. Sci. Data*, 9, 363–387, <https://doi.org/10.5194/essd-9-363-2017>, 2017.
- Lamping, N., Müller, J., Esper, O., Hillenbrand, C.-D., Smith, J. A., and Kuhn, G.: Highly branched isoprenoids reveal onset of deglaciation followed by dynamic sea-ice conditions in the western Amundsen Sea, Antarctica, *Quaternary. Sci. Rev.*, 228, 106103, <https://doi.org/10.1016/j.quascirev.2019.106103>, 2020.
- Lamping, N., Müller, J., Hefter, J., Mollenhauer, G., Haas, C., Shi, X., Vorrath, M.-E., and Lohmann, G.: Biomarker concentrations in marine surface sediment samples from West Antarctic continental shelves alongside satellite observations and model simulations, PANGAEA [data set], <https://doi.org/10.1594/PANGAEA.932265>, 2021.

- Lange, M., Ackley, S., Wadhams, P., Dieckmann, G., and Eicken, H.: Development of sea ice in the Weddell Sea, *Ann. Glaciol.*, 12, 92–96, 1989.
- Langhorne, P., Hughes, K., Gough, A., Smith, I., Williams, M., Robinson, N., Stevens, C., Rack, W., Price, D., and Leonard, G.: Observed platelet ice distributions in Antarctic sea ice: An index for ocean-ice shelf heat flux, *Geophys. Res. Lett.*, 42, 5442–5451, 2015.
- Leventer, A.: The fate of Antarctic “sea ice diatoms” and their use as paleoenvironmental indicators, *Antarctic sea ice. Biological processes, Interactions and Variability*, 73, 121–137, <https://doi.org/10.1029/AR073>, 1998.
- Li, X., Holland, D. M., Gerber, E. P., and Yoo, C.: Impacts of the north and tropical Atlantic Ocean on the Antarctic Peninsula and sea ice, *Nature*, 505, 538–542, 2014.
- Liu, R., Han, Z., Zhao, J., Zhang, H., Li, D., Ren, J., Pan, J., and Zhang, H.: Distribution and source of glycerol dialkyl glycerol tetraethers (GDGTs) and the applicability of GDGT-based temperature proxies in surface sediments of Prydz Bay, East Antarctica, *Polar Research*, 3557, <https://doi.org/10.33265/polar.v39.3557>, 2020.
- Locarnini, R. A., Mishonov, A. V., Antonov, J. I., Boyer, T. P., Garcia, H. E., Baranova, O. K., Zweng, M. M., Paver, C. R., Reagan, J. R., and Johnson, D. R.: World ocean atlas 2013. Volume 1, Temperature, NOAA Atlas NESDIS 73, 1, 40 pp., <https://doi.org/10.7289/V55X26VD>, 2013.
- Lohmann, G., Butzin, M., Eissner, N., Shi, X., and Stepanek, C.: Abrupt climate and weather changes across time scales, *Paleoceanography and Paleoclimatology*, 35, e2019PA003782, <https://doi.org/10.1029/2019PA003782>, 2020.
- López-García, P., Rodríguez-Valera, F., Pedrós-Alió, C., and Moreira, D.: Unexpected diversity of small eukaryotes in deep-sea Antarctic plankton, *Nature*, 409, 603–607, 2001.
- Lorenz, S. J. and Lohmann, G.: Acceleration technique for Milankovitch type forcing in a coupled atmosphere-ocean circulation model: method and application for the Holocene, *Clim. Dynam.*, 23, 727–743, 2004.
- Lott, F.: Alleviation of stationary biases in a GCM through a mountain drag parameterization scheme and a simple representation of mountain lift forces, *Mon. Weather. Rev.*, 127, 788–801, 1999.
- Loveland, T. R., Reed, B. C., Brown, J. F., Ohlen, D. O., Zhu, Z., Yang, L., and Merchant, J. W.: Development of a global land cover characteristics database and IGBP DISCover from 1 km AVHRR data, *Int. J. Remote Sens.*, 21, 1303–1330, 2000.
- Lü, X., Liu, X.-L., Elling, F. J., Yang, H., Xie, S., Song, J., Li, X., Yuan, H., Li, N., and Hinrichs, K.-U.: Hydroxylated isoprenoid GDGTs in Chinese coastal seas and their potential as a paleotemperature proxy for mid-to-low latitude marginal seas, *Org. Geochem.*, 89–90, 31–43, 2015.
- Massé, G., Belt, S. T., Crosta, X., Schmidt, S., Snape, I., Thomas, D. N., and Rowland, S. J.: Highly branched isoprenoids as proxies for variable sea ice conditions in the Southern Ocean, *Antarct. Sci.*, 23, 487–498, 2011.
- Massom, R. A., Scambos, T. A., Bennetts, L. G., Reid, P., Squire, V. A., and Stammerjohn, S. E.: Antarctic ice shelf disintegration triggered by sea ice loss and ocean swell, *Nature*, 558, 383–389, 2018.
- Mathiot, P., Goosse, H., Fichefet, T., Barnier, B., and Gallée, H.: Modelling the seasonal variability of the Antarctic Slope Current, *Ocean Sci.*, 7, 455–470, <https://doi.org/10.5194/os-7-455-2011>, 2011.
- Medlin, L.: *Berkeleya* spp. from Antarctic waters, including *Berkeleya adeliensis*, sp. nov., a new tube dwelling diatom from the undersurface of sea-ice, *Nova. Hedwigia.*, 100, 77–89, 1990.
- Meredith, M. P., Woodworth, P. L., Chereskin, T. K., Marshall, D. P., Allison, L. C., Bigg, G. R., Donohue, K., Heywood, K. J., Hughes, C. W., and Hibbert, A.: Sustained monitoring of the Southern Ocean at Drake Passage: Past achievements and future priorities, *Rev. Geophys.*, 49, RG4005, <https://doi.org/10.1029/2010RG000348>, 2011.
- Meyers, P. A.: Organic geochemical proxies of paleoceanographic, paleolimnologic, and paleoclimatic processes, *Org. Geochem.*, 27, 213–250, 1997.
- Moore, J. K. and Abbott, M. R.: Surface chlorophyll concentrations in relation to the Antarctic Polar Front: seasonal and spatial patterns from satellite observations, *J. Marine. Syst.*, 37, 69–86, 2002.
- Müller, J. and Stein, R.: High-resolution record of late glacial and deglacial sea ice changes in Fram Strait corroborates ice–ocean interactions during abrupt climate shifts, *Earth. Planet. Sc. Lett.*, 403, 446–455, 2014.
- Müller, J., Wagner, A., Fahl, K., Stein, R., Prange, M., and Lohmann, G.: Towards quantitative sea ice reconstructions in the northern North Atlantic: A combined biomarker and numerical modelling approach, *Earth. Planet. Sc. Lett.*, 306, 137–148, 2011.
- Nakayama, Y., Menemenlis, D., Zhang, H., Schodlok, M., and Rignot, E.: Origin of Circumpolar Deep Water intruding onto the Amundsen and Bellingshausen Sea continental shelves, *Nat. Commun.*, 9, 3403, <https://doi.org/10.1038/s41467-018-05813-1>, 2018.
- Nicholls, K. W., Østerhus, S., Makinson, K., Gammelsrød, T., and Fahrbach, E.: Ice-ocean processes over the continental shelf of the southern Weddell Sea, Antarctica: A review, *Rev. Geophys.*, 47, RG3003, <https://doi.org/10.1029/2007RG000250>, 2009.
- Nichols, P. D., Palmisano, A. C., Volkman, J. K., Smith, G. A., and White, D. C.: Occurrence of an isoprenoid C₂₅ diunsaturated alkene and high neutral lipid content in Antarctic sea-ice diatom communities 1, *J. Phycol.*, 24, 90–96, 1988.
- Nielsdóttir, M. C., Bibby, T. S., Moore, C. M., Hinz, D. J., Sanders, R., Whitehouse, M., Korb, R., and Achterberg, E. P.: Seasonal and spatial dynamics of iron availability in the Scotia Sea, *Mar. Chem.*, 130, 62–72, 2012.
- Nolting, R., De Baar, H., Van Bennekom, A., and Masson, A.: Cadmium, copper and iron in the Scotia Sea, Weddell Sea and Weddell/Scotia confluence (Antarctica), *Mar. Chem.*, 35, 219–243, 1991.
- Orsi, A. H., Whitworth III, T., and Nowlin Jr, W. D.: On the meridional extent and fronts of the Antarctic Circumpolar Current, *Deep-Sea Res. Pt. I.*, 42, 641–673, 1995.
- Otto-Bliesner, B. L., Braconnot, P., Harrison, S. P., Lunt, D. J., Abe-Ouchi, A., Albani, S., Bartlein, P. J., Capron, E., Carlson, A. E., Dutton, A., Fischer, H., Goelzer, H., Govin, A., Haywood, A., Joos, F., LeGrande, A. N., Lipscomb, W. H., Lohmann, G., Mahowald, N., Nehrbaas-Ahles, C., Pausata, F. S. R., Peter-schmitt, J.-Y., Phipps, S. J., Renssen, H., and Zhang, Q.: The PMIP4 contribution to CMIP6 – Part 2: Two interglacials, scientific objective and experimental design for Holocene and Last

- Interglacial simulations, *Geosci. Model Dev.*, 10, 3979–4003, <https://doi.org/10.5194/gmd-10-3979-2017>, 2017.
- Otto-Bliesner, B. L., Brady, E. C., Zhao, A., Brierley, C. M., Axford, Y., Capron, E., Govin, A., Hoffman, J. S., Isaacs, E., Kageyama, M., Scussolini, P., Tzedakis, P. C., Williams, C. J. R., Wolff, E., Abe-Ouchi, A., Braconnot, P., Ramos Buarque, S., Cao, J., de Vernal, A., Guarino, M. V., Guo, C., LeGrande, A. N., Lohmann, G., Meissner, K. J., Menviel, L., Morozova, P. A., Nisancioglu, K. H., O’ishi, R., Salas y Méliá, D., Shi, X., Sicard, M., Sime, L., Stepanek, C., Tomas, R., Volodin, E., Yeung, N. K. H., Zhang, Q., Zhang, Z., and Zheng, W.: Large-scale features of Last Interglacial climate: results from evaluating the *lig127k* simulations for the Coupled Model Intercomparison Project (CMIP6)–Paleoclimate Modeling Intercomparison Project (PMIP4), *Clim. Past*, 17, 63–94, <https://doi.org/10.5194/cp-17-63-2021>, 2021.
- Park, E., Hefter, J., Fischer, G., Iversen, M. H., Ramondenc, S., Nöthig, E.-M., and Mollenhauer, G.: Seasonality of archaeal lipid flux and GDGT-based thermometry in sinking particles of high-latitude oceans: Fram Strait (79° N) and Antarctic Polar Front (50° S), *Biogeosciences*, 16, 2247–2268, <https://doi.org/10.5194/bg-16-2247-2019>, 2019.
- Parkinson, C. L.: A 40 y record reveals gradual Antarctic sea ice increases followed by decreases at rates far exceeding the rates seen in the Arctic, *P. Natl. Acad. Sci. USA.*, 116, 14414–14423, 2019.
- Parkinson, C. L. and Cavalieri, D. J.: Antarctic sea ice variability and trends, 1979–2010, *The Cryosphere*, 6, 871–880, <https://doi.org/10.5194/tc-6-871-2012>, 2012.
- Paul, S., Willmes, S., and Heinemann, G.: Long-term coastal-polynya dynamics in the southern Weddell Sea from MODIS thermal-infrared imagery, *The Cryosphere*, 9, 2027–2041, <https://doi.org/10.5194/tc-9-2027-2015>, 2015.
- Pritchard, H., Ligtenberg, S., Fricker, H., Vaughan, D., Van den Broeke, M., and Padman, L.: Antarctic ice-sheet loss driven by basal melting of ice shelves, *Nature*, 484, 502–505, 2012.
- Raddatz, T., Reick, C., Knorr, W., Kattge, J., Roeckner, E., Schnur, R., Schnitzler, K.-G., Wetzell, P., and Jungclaus, J.: Will the tropical land biosphere dominate the climate–carbon cycle feedback during the twenty-first century?, *Clim. Dynam.*, 29, 565–574, 2007.
- Riaux-Gobin, C. and Poulin, M.: Possible symbiosis of *Berkeleya adeliensis* Medlin, *Synedropsis fragilis* (Manguin) Hasle et al. and *Nitzschia lecontei* Van Heurck (Bacillariophyta) associated with land-fast ice in Adélie Land, Antarctica, *Diatom. Res.*, 19, 265–274, 2004.
- Riaux-Gobin, C., Dieckmann, G. S., Poulin, M., Neveux, J., Labruno, C., and Vétion, G.: Environmental conditions, particle flux and sympagic microalgal succession in spring before the sea-ice break-up in Adélie Land, East Antarctica, *Polar Res.*, 32, 19675, <https://doi.org/10.3402/polar.v32i0.19675>, 2013.
- Rignot, E., Mouginot, J., Scheuchl, B., Van Den Broeke, M., Van Wessem, M. J., and Morlighem, M.: Four decades of Antarctic Ice Sheet mass balance from 1979–2017, *P. Natl. Acad. Sci. USA.*, 116, 1095–1103, 2019.
- Rintoul, S., Hughes, C., and Olbers, D.: The Antarctic circumpolar current system, *International Geophysics*, 77, 271–302, [https://doi.org/10.1016/S0074-6142\(01\)80124-8](https://doi.org/10.1016/S0074-6142(01)80124-8), 2001.
- Roeckner, E., Dümenil, L., Kirk, E., Lunkeit, F., Ponater, M., Rockel, B., Sausen, R., and Schlese, U.: The Hamburg version of the ECMWF model (ECHAM), Research activities in atmospheric and oceanic modelling, CAS/JSC Working Group on Numerical Experimentation, 13, 7.1–7.4, 1989.
- Rontani, J.-F., Belt, S. T., and Amiraux, R.: Biotic and abiotic degradation of the sea ice diatom biomarker IP25 and selected algal sterols in near-surface Arctic sediments, *Organic Geochemistry* 118, 73–88, 2018.
- Rontani, J.-F., Smik, L., and Belt, S. T.: Autoxidation of the sea ice biomarker proxy IPSO25 in the near-surface oxic layers of Arctic and Antarctic sediments, *Organic Geochemistry*, 129, 63–76, 2019.
- Sangrà, P., Gordo, C., Hernández-Arencibia, M., Marrero-Díaz, A., Rodríguez-Santana, A., Stegner, A., Martínez-Marrero, A., Pelegrí, J. L., and Pichon, T.: The Bransfield current system, *Deep-Sea Res. Pt. I.*, 58, 390–402, 2011.
- Scambos, T. A., Bell, R. E., Alley, R. B., Anandakrishnan, S., Bromwich, D., Brunt, K., Christianson, K., Creyts, T., Das, S., and DeConto, R.: How much, how fast?: A science review and outlook for research on the instability of Antarctica’s Thwaites Glacier in the 21st century, *Global. Planet. Change.*, 153, 16–34, 2017.
- Schlitzer, R.: Ocean Data View, ODV [data set], available at: <https://odv.awi.de/> (last access: August 2021), 2017.
- Schmidt, K., Brown, T. A., Belt, S. T., Ireland, L. C., Taylor, K. W. R., Thorpe, S. E., Ward, P., and Atkinson, A.: Do pelagic grazers benefit from sea ice? Insights from the Antarctic sea ice proxy IPSO25, *Biogeosciences*, 15, 1987–2006, <https://doi.org/10.5194/bg-15-1987-2018>, 2018.
- Schmidtko, S., Heywood, K. J., Thompson, A. F., and Aoki, S.: Multidecadal warming of Antarctic waters, *Science*, 346, 1227–1231, 2014.
- Schofield, O., Brown, M., Kohut, J., Nardelli, S., Saba, G., Waite, N., and Ducklow, H.: Changes in the upper ocean mixed layer and phytoplankton productivity along the West Antarctic Peninsula, *Philos. T. R. Soc. A*, 376, 20170173, <https://doi.org/10.1098/rsta.2017.0173>, 2018.
- Schouten, S., Hopmans, E. C., Schefuß, E., and Damsté, J. S. S.: Distributional variations in marine crenarchaeotal membrane lipids: a new tool for reconstructing ancient sea water temperatures?, *Earth. Planet. Sc. Lett.*, 204, 265–274, 2002.
- Schouten, S., Hopmans, E. C., and Damsté, J. S. S.: The organic geochemistry of glycerol dialkyl glycerol tetraether lipids: A review, *Organic Geochemistry*, 54, 19–61, 2013.
- Schröder, M.: The Expedition PS111 of the Research POLARSTERN to the southern Weddell Sea in 2018, *Berichte zur Polar-und Meeresforschung (Reports on Polar and Marine Research)*, Alfred Wegener Institute for Polar and Marine Research, Bremerhaven, Germany, 718, 161 pp., 2018.
- Sidorenko, D., Goessling, H., Koldunov, N., Scholz, P., Danilov, S., Barbi, D., Cabos, W., Gurses, O., Harig, S., and Hinrichs, C.: Evaluation of FESOM2.0 coupled to ECHAM6.3: Preindustrial and HighResMIP simulations, *J. Adv. Model. Earth. Sy.*, 11, 3794–3815, 2019.
- Smik, L., Belt, S. T., Lieser, J. L., Armand, L. K., and Leventer, A.: Distributions of highly branched isoprenoid alkenes and other algal lipids in surface waters from East Antarctica: further insights for biomarker-based paleo sea-ice reconstruction, *Organic Geochemistry*, 95, 71–80, 2016.

- Smith, J. A., Hillenbrand, C.-D., Kuhn, G., Larter, R. D., Graham, A. G. C., Ehrmann, W., Moreton, S. G., and Forwick, M.: Deglacial history of the West Antarctic Ice Sheet in the western Amundsen Sea Embayment, *Quaternary Sci. Rev.*, 30, 488–505, 2011.
- Smith, J. A., Hillenbrand, C.-D., Kuhn, G., Klages, J. P., Graham, A. G. C., Larter, R. D., Ehrmann, W., Moreton, S. G., Wiers, S., and Frederichs, T.: New constraints on the timing of West Antarctic Ice Sheet retreat in the eastern Amundsen Sea since the Last Glacial Maximum, *Glob. Planet. Change.*, 112, 224–237, 2014.
- Smith, J. A., Andersen, T., Shortt, M., Gaffney, A., Truffer, M., Stanton, T. P., Bindschadler, R., Dutrieux, P., Jenkins, A., and Hillenbrand, C.-D.: Sub-ice-shelf sediments record history of twentieth-century retreat of Pine Island Glacier, *Nature*, 541, 77–80, 2017.
- Spencer-Jones, C. L., McClymont, E. L., Bale, N. J., Hopmans, E. C., Schouten, S., Müller, J., Abrahamsen, E. P., Allen, C., Bickert, T., Hillenbrand, C.-D., Mawbey, E., Peck, V., Svalova, A., and Smith, J. A.: Archaeal intact polar lipids in polar waters: a comparison between the Amundsen and Scotia seas, *Biogeosciences*, 18, 3485–3504, <https://doi.org/10.5194/bg-18-3485-2021>, 2021.
- Stevens, B., Giorgetta, M., Esch, M., Mauritsen, T., Crueger, T., Rast, S., Salzmann, M., Schmidt, H., Bader, J., and Block, K.: Atmospheric component of the MPI-M Earth system model: ECHAM6, *J. Adv. Model. Earth. Sy.*, 5, 146–172, 2013.
- Stocker, T. F., Qin, D., Plattner, G.-K., Tignor, M., Allen, S. K., Boschung, J., Nauels, A., Xia, Y., Bex, V., and Midgley, P. M.: The physical science basis. Contribution of working group I to the fifth assessment report of the intergovernmental panel on climate change, *Computational Geometry*, 18, 95–123, 2013.
- Thomas, D. N. (Ed.): *Sea ice*, 3rd edn., John Wiley and Sons, USA, 2017.
- Thompson, A. F., Heywood, K. J., Thorpe, S. E., Renner, A. H., and Trasviña, A.: Surface circulation at the tip of the Antarctic Peninsula from drifters, *J. Phys. Oceanogr.*, 39, 3–26, 2009.
- Thompson, A. F., Stewart, A. L., Spence, P., and Heywood, K. J.: The Antarctic Slope Current in a changing climate, *Rev. Geophys.*, 56, 741–770, 2018.
- Turner, J., Orr, A., Gudmundsson, G. H., Jenkins, A., Bingham, R. G., Hillenbrand, C.-D., and Bracegirdle, T. J.: Atmosphere-ocean-ice interactions in the Amundsen Sea Embayment, West Antarctica, *Rev. Geophys.*, 55, 235–276, 2017.
- Turner, J., Guarino, M. V., Arnatt, J., Jena, B., Marshall, G. J., Phillips, T., Bajish, C. C., Clem, K., Wang, Z., Andersson, T., Murphy, E. J., and Cavanagh, R.: Recent Decrease of Summer Sea Ice in the Weddell Sea, Antarctica, *Geophys. Res. Lett.*, 47, e2020GL087127, <https://doi.org/10.1029/2020GL087127>, 2020.
- Valcke, S.: The OASIS3 coupler: a European climate modelling community software, *Geosci. Model Dev.*, 6, 373–388, <https://doi.org/10.5194/gmd-6-373-2013>, 2013.
- Vaughan, D. G.: West Antarctic Ice Sheet collapse – the fall and rise of a paradigm, *Climatic Change*, 91, 65–79, 2008.
- Vaughan, D. G., Marshall, G. J., Connolley, W. M., Parkinson, C., Mulvaney, R., Hodgson, D. A., King, J. C., Pudsey, C. J., and Turner, J.: Recent rapid regional climate warming on the Antarctic Peninsula, *Climatic Change*, 60, 243–274, 2003.
- Vernet, M., Geibert, W., Hoppema, M., Brown, P. J., Haas, C., Hellmer, H., Jokat, W., Jullion, L., Mazloff, M., and Bakker, D.: The Weddell Gyre, Southern Ocean: present knowledge and future challenges, *Rev. Geophys.*, 57, 623–708, 2019.
- Volkman, J. K.: Lipid markers for marine organic matter, in: *Marine organic matter: Biomarkers, isotopes and DNA*, Springer Verlag, Berlin Heidelberg, 27–70, 2006.
- Vorrath, M.-E., Müller, J., Esper, O., Mollenhauer, G., Haas, C., Schefuß, E., and Fahl, K.: Highly branched isoprenoids for Southern Ocean sea ice reconstructions: a pilot study from the Western Antarctic Peninsula, *Biogeosciences*, 16, 2961–2981, <https://doi.org/10.5194/bg-16-2961-2019>, 2019.
- Vorrath, M.-E., Müller, J., Rebolledo, L., Cárdenas, P., Shi, X., Esper, O., Opel, T., Geibert, W., Muñoz, P., Haas, C., Kuhn, G., Lange, C. B., Lohmann, G., and Mollenhauer, G.: Sea ice dynamics in the Bransfield Strait, Antarctic Peninsula, during the past 240 years: a multi-proxy intercomparison study, *Clim. Past*, 16, 2459–2483, <https://doi.org/10.5194/cp-16-2459-2020>, 2020.
- Wang, Z., Turner, J., Wu, Y., and Liu, C.: Rapid Decline of Total Antarctic Sea Ice Extent during 2014–16, Controlled by Wind-Driven Sea Ice Drift, *J. Climate*, 32, 5381–5395, 2019.
- Witus, A. E., Branecky, C. M., Anderson, J. B., Szczuciński, W., Schroeder, D. M., Blankenship, D. D., and Jakobsson, M.: Meltwater intensive glacial retreat in polar environments and investigation of associated sediments: example from Pine Island Bay, West Antarctica, *Quaternary. Sci. Rev.*, 85, 99–118, 2014.
- Zamelczyk, K., Rasmussen, T. L., Husum, K., Hafliðason, H., de Vernal, A., Ravna, E. K., Hald, M., and Hillaire-Marcel, C.: Paleoceanographic changes and calcium carbonate dissolution in the central Fram Strait during the last 20 ka, *Quaternary. Res.*, 78, 405–416, 2012.
- Zielinski, U., Gersonde, R., Sieger, R., and Fütterer, D.: Quaternary surface water temperature estimations: Calibration of a diatom transfer function for the Southern Ocean, *Paleoceanography and Paleoclimatology*, 13, 365–383, 1998.
- Zwally, H. J., Comiso, J. C. C., Parkinson, L., Campbell, W. J., Carsey, F. D., and P. Gloersen: Antarctic sea-ice, 1973–1976: Satellite passive-microwave observations., NASA Spec. Publ., Washington D. C., USA, 459 pp., 1983.